Biosystems Engineering 258 (2025) 104255

Contents lists available at ScienceDirect

Biosystems Engineering

journal homepage: www.elsevier.com/locate/www.elsevier.com/locate/issn/15375110

Research Paper

Modelling machine-induced soil deformation in forest soils using stump proximity and machine learning

Gunta Grube [a,b,*], Stefano Grigolato [a,b], Jari Ala-Ilomäki [c], Johanna Routa [d], Harri Lindeman [e], Rasmus Astrup [f], Bruce Talbot [b]

[a] Department of Land, Environment, Agriculture and Forestry (TESAF), University of Padova, Viale dell'Università 16, 35020 Legnaro, Padova, Italy
[b] Department of Forest and Wood Science, Stellenbosch University, Paul Sauer Building, Bosman St, 7599 Stellenbosch, South Africa
[c] Natural Resources Institute Finland (Luke), Latokartanonkaari 9, 00790 Helsinki, Finland
[d] Natural Resources Institute Finland (Luke), Yliopistokatu 6B, 80100 Joensuu, Finland
[e] Natural Resources Institute Finland (Luke), Tekniikankatu 1, 33720 Tampere, Finland
[f] Norwegian Institute of Bioeconomy Research (NIBIO), Høgskoleveien 8, 1433 Ås, Norway

ARTICLE INFO

Keywords:
Root reinforcement
Soil compaction
Machine traffic
UAV
Machine learning

ABSTRACT

Soil deformation is a key challenge in sustainable timber harvesting, particularly in environments with low bearing capacity. In mechanised forestry, this issue is especially pronounced in peatlands, where rutting arises from soil displacement and root shearing within the soft, organic substrate. While tree roots are known to reinforce soil, the specific role of stump-root systems in mitigating rut formation remains underexplored. This study examines the influence of stump presence on rut depth using Unmanned Aerial Vehicle (UAV) based digital terrain models (DTMs), manual field measurements, spatial modelling, and machine learning techniques. UAV-derived rut depth estimates were first compared with manual data, revealing slightly lower values in deeper ruts, particularly in curved trails, with mean discrepancies of 3 cm. Statistical analysis confirmed that cumulative stump influence significantly reduced rut depth, with a small to medium effect in straight trails (ε^2 = 0.04–0.20) and a moderate to large effect in curved trails (ε^2 = 0.02–0.32). Machine learning models achieved high predictive accuracy (R^2 = 0.69–0.85), identifying stump-related variables and soil shear modulus as key predictors of rut formation. These findings emphasise the importance of incorporating stump-root reinforcement into forest planning to optimise machine path selection and minimise soil disturbance. Future research should refine species-specific reinforcement models and explore advanced root mapping techniques, such as ground-penetrating radar (GPR), to strengthen decision-support tools for sustainable forestry.

Science4Impact statement (S4IS)

This study presents a spatially informed methodology to evaluate the influence of tree stump-root systems on rut formation in peatland soils. By integrating UAV mapping and machine learning, this study enables the predictive identification of low-impact areas, reducing site disturbance and supporting climate-smart forestry. These findings offer a practical starting point and a potential tool for optimising skid trail layout, improving operational efficiency, and minimising soil disturbance and site damage. The approach supports evidence-based decision-making in peatland conservation, helping align forest operations with broader environmental and climate goals.

1. Introduction

Forests are a key source of renewable resources, essential for timber production and economic sustainability (Favero et al., 2020; Grassi et al., 2017). The increasing demand for sustainably sourced timber has intensified efforts to optimise wood mobilisation while ensuring long-term ecological balance (Blattert et al., 2023; Lerink et al., 2023).

* Corresponding author at: Department of Land, Environment, Agriculture and Forestry (TESAF), University of Padova, Viale dell'Università 16, 35020 Legnaro, Padova, Italy.
E-mail addresses: gunta.grube@unipd.it (G. Grube), stefano.grigolato@unipd.it (S. Grigolato), jari.ala-ilomaki@luke.fi (J. Ala-Ilomäki), johanna.routa@luke.fi (J. Routa), harri.lindeman@luke.fi (H. Lindeman), rasmus.astrup@nibio.no (R. Astrup), bruce@sun.ac.za (B. Talbot).

https://doi.org/10.1016/j.biosystemseng.2025.104255
Received 17 April 2025; Received in revised form 29 July 2025; Accepted 1 August 2025
Available online 27 August 2025

Nomenclature

Abbreviations

Abbreviation	Definition
CI	Cumulative influence (of stumps)
CSF	Cloth simulation filter
DTM	Digital terrain model
DTW	Depth-to-water
GCP	Ground control point
GPR	Ground-penetrating radar
GNSS	Global navigation satellite system
ICP	Iterative closest point
MAE	Mean absolute error
NGP	Nominal ground pressure
RAR	Root area ratio
RD	Rut depth
RF	Random forest
RFE	Recursive feature elimination
RMSE	Root mean square error
RTK	Real-Time kinematic
RRV	Root reinforcement value
SD	Standard deviation
SfM	Structure from Motion
UAV	Unmanned aerial vehicle

Latin Symbols

Symbol	Definition	Unit
d	Distance from pixel to stump	m
D	Stump diameter	m
D_{ave}	Average stump diameter	m
G_{trail}	Shear modulus of the trail	kPa
$I(d)$	Influence at distance d	arbitrary units
L	Max reinforcement (sigmoid model)	kPa
R^2	Coefficient of determination	–
R_{final}	Total root reinforcement	arbitrary units
R_{norm}	Normalised root reinforcement	% arbitrary units (0–100)
S_{peat}	Estimated peat shear strength	kPa
W_{peat}	Peat moisture content ($\%_{wgt}$)	%
x, y	Spatial coordinates	m
x_0	Sigmoid inflection point	m
y_i	Observed rut depth	cm, m
$\hat{y}_i$	Predicted rut depth	cm, m

Greek Symbols

Symbol	Definition	Unit
α	Scaling constant for stump diameter effect	–
ϵ^2	Epsilon squared, effect size (Kruskal–Wallis)	–
κ	Decay constant (influence model) and steepness (logistic)	–
μ	Mean in SD and R^2 formula	–
σ	Standard deviation	cm

In many parts of Northern Europe, the Baltic states, and Russia, a substantial share of timber production takes place on organically rich soils, including peatlands. Such soils are widespread across these regions and characterised by high organic matter content (Piirainen et al., 2017).

Peatland ecosystems are known for their high carbon storage capacity and waterlogged conditions (Loisel & Gallego-Sala, 2022), which pose unique challenges for timber production. Historically, peatlands have often been managed through drainage to increase forest productivity and timber supply, thereby supporting tree growth and facilitating easier harvesting processes (Turunen & Valpola, 2020). It is estimated that approximately 15 million hectares (Mha) of peatlands have been drained for forestry purposes in the temperate and boreal regions, with about 10 Mha in the Baltic Sea Region (Finland, Sweden, Estonia, Latvia, Lithuania, and parts of Russia) alone (Paavilainen & Päivänen, 1995; Piirainen et al., 2017). For instance, in Finland, peatlands cover approximately 8.8 Mha, accounting for 33% of forestry land, with slightly more than half (4.6 Mha) being drained for forestry. These drained peatlands contribute significantly to timber production, accounting for 25% of the total annual stem volume increment of 104 Mm^3, with a mean annual increment of 4.6 $m^3\ ha^{-1}$ (Peltola, 2014). The share of managed peatland forests is highest in southern and eastern Finland, where 88–90% of the peatland area has been drained, compared with only about 23% in Lapland, the northernmost region of Finland (Turunen & Valpola, 2020).

Despite their economic importance, drained peatlands present significant challenges for forestry operations due to their distinct physical and ecological characteristics, such as low bulk density and high porosity (Laine et al., 2006). Unlike mineral soils, peatlands are composed primarily of accumulated organic material, formed over thousands of years under water-saturated, oxygen-poor conditions (Paavilainen & Päivänen, 1995). This results in a multi-layered structure, typically consisting of a surface layer (*acrotelm*) that is up to several decimeters thick. This layer is porous and highly permeable to water, containing living mosses, roots, and decomposing organic material. The deeper or sub-surface layer (*catotelm*) consists of variably decomposed, waterlogged peat with very low shear strength (Paavilainen & Päivänen, 1995; Sallinen et al., 2019; Similä et al., 2014).

Peat deposits vary in thickness, with boreal forested peatlands typically having an organic layer exceeding 30 cm (Paavilainen & Päivänen, 1995; Sallinen et al., 2019; Zoltai et al., 1996). As the peat depth increases, its bearing capacity decreases, making the soil highly susceptible to deformation under external loads (Lepilin et al., 2022; Prinz et al., 2023). When heavy forestry machinery moves across these soft, saturated soils, the high ground pressure, combined with low structural integrity, results in soil displacement, compaction, and rut formation (Ala-Ilomäki et al., 2011). These disturbances are particularly severe under poor trafficability conditions, where repeated machine passes may destabilise the peat even more (Niemi et al., 2017; Uusitalo & Ala-Ilomäki, 2013; Vega-Nieva et al., 2009), leading to long-term soil degradation, hydrological disruption, and reduced tree growth.

Research has shown that rut formation is strongly influenced by soil strength, traffic frequency, and trail design, with deeper ruts forming as shear strength decreases and the number of machine passes increases (Ala-Ilomäki et al., 2021; Solgi et al., 2018; Uusitalo et al., 2015). Forwarders equipped with wider trails or additional wheels help mitigate rut depth by distributing ground pressure more effectively. For instance, trials with 700 mm wide tyres showed a significant reduction in rut depth compared to 600 mm configurations under equivalent loads (Neri et al., 2007).

However, while they reduce rutting during the early machine passes, rut formation still progresses with repeated traffic, particularly on soft soils, where continued compaction and displacement occur (Breinig et al., 2025; Brennensthul et al., 2024). Trail design also plays a role, as wider trails (6 m) allow operators to avoid

deepening existing ruts, though further widening beyond this offers little additional benefit (Uusitalo et al., 2015). Furthermore, modern forwarders are more favourable in minimising rut formation compared to lighter forwarders from the 1980s, likely due to the use of bogie axles in the front and improved trail design, which helps distribute weight more effectively and reduce soil pressure (Ala-Ilomäki et al., 2011).

In recent years, to enhance insight into soil disturbance caused by forestry machinery, numerous studies have explored the application of remote sensing techniques, particularly UAV-based photogrammetry and machine learning. Drone-based measurements provide highly accurate rut depth estimations, closely matching manual measurements while enabling large-scale, efficient assessments (Marra et al., 2021). Deep learning (DL) applied to UAV imagery provided an accuracy of 79.5% for detecting ruts, with the highest precision for severe rutting (Bhatnagar et al., 2022). Additionally, Depth-to-Water (DTW) maps help predict rut severity, with 71% of severe ruts occurring in areas with DTW values below 1 m (Heppelmann et al., 2022).

While these advances in remote sensing improve the ability to monitor rut formation, they do not address the underlying factors that influence soil resistance to deformation. One critical but often overlooked aspect is the role of root systems in reinforcing soil mechanical strength. Roots improve soil stability through tensile resistance, root-soil interlocking, and mechanical support, which together increase shear resistance, distribute stress, and bind soil particles (Coutts, 1983; Schwarz et al., 2013; Wästerlund, 1989). These factors directly influence the soil's shear modulus, which quantifies its resistance to deformation, which determines its structural integrity and ability to resist rut formation (Ala-Ilomäki, 2013). Because roots contribute to shear strength, they also play a fundamental role in soil reinforcement, with their effectiveness depending on factors such as root density, root distribution, and tensile strength (Schwarz et al., 2010).

These characteristics differ among tree species and soil types, resulting in variations in root reinforcement values (Kalliokoski, 2011). In boreal forests of Finland, Sweden, and the Baltic states, the dominant species — Scots pine (*Pinus sylvestris*) and Norway spruce (*Picea abies*) both contribute to soil reinforcement, but in different ways. Scots pine typically develops a deep root system with strong tap roots, improving stability in mineral soils. However, on wet peatlands, it may also adopt a shallower root structure. Norway spruce, on the other hand, has a shallower, plate-like root system that reinforces the upper peat layer (Kalliokoski, 2011; Stokes & Mattheck, 1996).

Root reinforcement is typically evaluated using empirical or mechanistic models that assess how roots contribute to soil stability (Schwarz et al., 2010). Most studies in recent decades have followed the approach of Waldron (1977), Wu et al. (1979), which treat root bundles as adding cohesion to the soil. These models require parameters such as root tensile strength, root area ratio (RAR), and root distribution, obtained through field and laboratory tests (Genet et al., 2005; Schwarz et al., 2010). While advanced models such as the Root Bundle Model with Weibull survival (RBMw) (Schwarz et al., 2013) and RootMap (Schwarz et al., 2010) improve predictions by incorporating progressive root failure, they primarily focus on slope stability and do not account for stump-root influence on soil response to machine traffic.

Some studies have attempted to quantify the spatial effects of stump-root systems (Piskunov, 2023) and have found that stumps help reduce rut depth variability along skidding trails. However, comprehensive spatial modelling approaches remain underdeveloped, and no existing model fully integrates stump-root reinforcement, soil properties, and machine loading into a predictive model. There is a clear need for predictive tools that support machine path planning, enabling managers and operators to avoid high-risk areas and minimise soil disturbance. Improved management strategies are also essential for optimising forestry operations on sensitive soils.

This study aims to address that gap by developing a spatially explicit model that integrates stump locations and characteristics, soil and environmental parameters, and machine-induced depth values. Specifically, this study aim to (a) evaluate the accuracy of UAV-based Digital Terrain Models (DTM) by comparing them with manual rut depth measurements and (b) develop a spatial decay model that interpolates stump diameter and root reinforcement effects over distance. Additionally, the study utilised machine learning model to assess key predictors of rut depth and evaluate how stump-related variables influence soil deformation in straight and curved trail configurations. By further integrating this approach with DTW maps, the model could improve decision-making in drained peatlands, reducing the environmental impact of forestry operations.

2. Materials and methods

2.1. Study area

The research was conducted in a peatland area near Tiilikkala in the municipality of Rautavaara, Northern Savonia, Finland (61° 32′ 0'' N, 26° 50′ 0'' E, UTM zone 35N) (Fig. 1). The Rautavaara region is considered generally flat, with elevations ranging from sea level to about 100 to 200 meters above sea level. The landscape is primarily natural, with vast peatlands, considerable forest areas, and numerous lakes, including the nearby Lake Pielinen (Similä et al., 2014).

The region is characterised by a cold temperate climate with considerable seasonal changes. Winters are long, cold, and snowy, while summers are mild and short. The average annual temperature is around 2 to 4 °C, with January being the coldest month (−10 to −15 °C) and July being the warmest month (15 to 20 °C). Rainfall is relatively evenly distributed throughout the year, averaging approximately 600–700 mm (Finnish Meteorological Institute, 2018).

The study site is a mixed stand dominated by Scots pine (*Pinus sylvestris*) and Norway spruce (*Picea abies*). Peat depth in the area averages 149 cm, with a moisture content of approximately 86%$_{wgt}$. The groundwater depth is relatively shallow, averaging approximately 29 cm.

2.2. Data collection and processing

2.2.1. Field data collection

The study area comprises five test trails, each with two configurations — straight and curved. In this context, the term ''trail'' refers to the machine's travel path, including both the left and right wheel ruts formed by the forwarder. The straight trails were 20 meters long and 4 meters wide, while the curved trails, also 4 meters wide, had a 20-meter radius and formed a 90° turn. The trails were carefully designed to allow the forwarders to move smoothly between straight and curved configurations without causing sharp turns or damaging the paths. To keep the soil and tree roots within the test trails undisturbed, the trails were prepared in advance using a harvester operating outside the test areas. Felled trees were processed away from the trails to avoid creating slash mats.

Five different models of forwarders were tested, each equipped with specific track configurations suited for the conditions. These forwarders were used consistently on both straight and curved configurations. The forwarders included — the Ponsse Elk with a long wheelbase (LWB), the older generation Ponsse Elk with Fomatec tracks (EFwo), the older generation Ponsse Elk with Fomatec tracks and add-on track shoes (EFw), the Ponsse Buffalo with KOPA high flotation tracks (Kopa), and the Ponsse Elk 10 W with Olofsfors mixed tracks (E10 W). The data used in this study were initially collected as part of a previous investigation on rut formation in peatlands (Ala-Ilomäki et al., 2021). For detailed specifications of the machines used, please refer to the original study.

UAV-based data collection was carried out at the same experimental sites and during the same 2019 field campaign, alongside the manual rut depth measurements. UAV images were captured immediately before and after each machine pass, ensuring that all data sources reflect

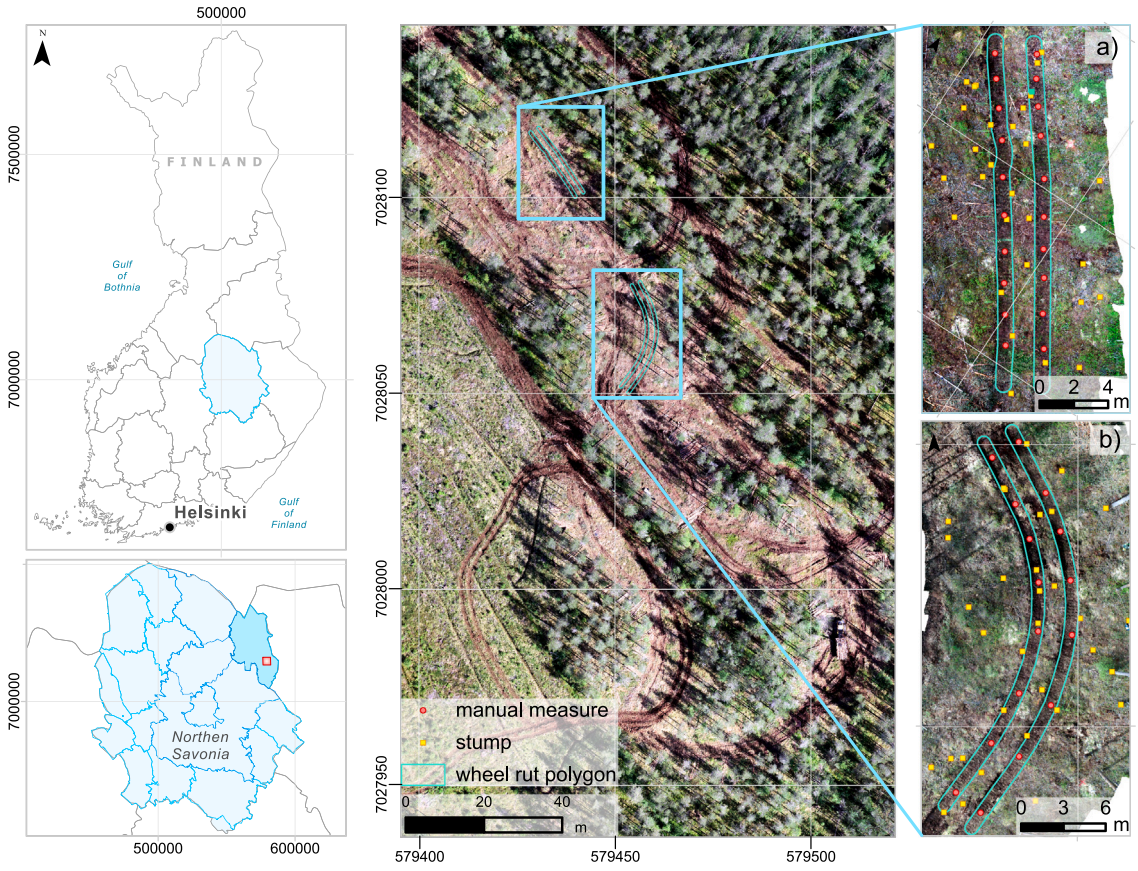

Fig. 1. Study area in a peatland near Tiilikkala, Rautavaara, Northern Savonia, Finland. The figure displays straight and curved sections of Trail 1 after the third machine pass. The left panel shows the site location, while the middle and right panels present orthomosaics of the trails. Red dots indicate manual rut depth measurements along the wheel ruts (blue polygons), and yellow dots mark tree stumps. This setup was used consistently across all five trails. (For interpretation of the references to colour in this figure legend, the reader is referred to the web version of this article.)

the same site conditions. As a result, no temporal changes needed to be considered between the different data collection methods.

The machine test mass includes the estimated load and the manufacturer-specified mass of the forwarder and tracks. The forwarder was loaded with approximately 5,100 kg of pulpwood, each piece averaging 4.56 meters in length. This load size, selected by the forwarder operator during the initial test, was chosen to facilitate three to four passes on each trail with minimal risk of bogging down. Consequently, the forwarder completed the planned number of passes on each trail.

Rut depth was measured after each forwarder pass using a horizontal laser level and a surveyor's measuring rod. Measurements were taken at specific points along both the right and left wheel ruts, generally spaced every 2–3 meters across the trails. A total of 198 measurements were collected — 126 from straight sections and 72 from curved sections, with the difference reflecting variations in trail length. Since straight sections were longer, they naturally yielded more total measurements. These measurements were distributed across all test trails to ensure a representative assessment of rut depth variability in both configurations. To maintain consistency, measurement points were marked on the peat surface using spray paint. This ensured that we recorded new data at the same locations throughout the passes.

Rut depth was recorded at the deepest point, typically within a track shoe depression in the peat. Additionally, peat moisture content (W_{peat}, %wgt) was recorded for each trail and configuration as a site-specific parameter. Shear modulus (G_{trail}, kPa), measured with a spiked shear vane (Ala-Ilomäki, 2013), was also recorded at each measurement point. Nominal ground pressure (NGP) was determined based on the machine's technical specifications and depended on both the contact area and the machine's weight. The front and rear track sections were reported separately to account for variations in load distribution. For further analysis, the average (NGP_{mean}) and maximum NGP (NGP_{max}) values were used to represent the technical specifications of the machines. Three passes, each defined as a single traversal of the machine in one direction, were conducted on trails 1, 3, and 4, while trails 2 and 5 underwent four passes. A fourth pass was not conducted at all sites because the peat had reached its strength limit.

2.2.2. UAV data collection and processing

Drone flights were conducted using the DJI Phantom 4 Pro (model: FC6310), flying at altitudes around 30-35 m, capturing images over the same trails before the operations and immediately after each machine pass. A total of fifty ground control points (GCPs) were recorded using a Real-Time Kinematic Global Navigation Satellite System (RTK-GNSS) device. Each trail configuration had at least three GCPs, with an average of 56 images captured per area.

The RGB images and GCPs were processed in Agisoft Metashape Professional (Agisoft, 2021) to generate an initial point cloud dataset for each trail and its configurations. Agisoft Metashape combines Structure-from-Motion (SfM) and photogrammetric stereo-matching algorithms for 3D reconstruction from unordered but overlapping imagery. The workflow included image import, alignment, georeferencing, and optimisation, followed by the generation of an initial point cloud. The GCPs were used to refine camera positions and improve georeferencing accuracy.

All point clouds were then exported in .LAS format for further processing. To ensure precise alignment across datasets, point clouds from each trail and pass were manually aligned in CloudCompare using the "Align (point pairs picking)" tool. At least seven point pairs were selected for point cloud registration, with the initial pre-operation dataset serving as the reference for aligning all subsequent point clouds.

Fine registration via the iterative closest point (ICP) algorithm was then applied to further improve dataset alignment (CloudCompare, 2024).

To remove irrelevant vegetation, point clouds were classified using the cloth simulation filter (CSF) in CloudCompare (Zhang et al., 2016). The filtering parameters, such as cloth resolution (1.5), maximum iterations (1000), and classification threshold (0.5), were determined through trial and error to best separate ground points from vegetation while preserving terrain features. The aligned and classified point clouds were then reimported into Agisoft Metashape, where orthomosaics were generated for each trail and configuration. Only points classified as 'ground' were used to generate a digital terrain model (DTM) at a resolution of 0.03 m. Finally, all DTMs and orthomosaics were exported in GeoTIFF (.tif) format.

2.2.3. Rut depth analysis

To quantify elevation changes caused by each machine pass and assess the accuracy of UAV-based rut depth measurements, we used DTMs to evaluate elevation differences after each pass. These changes were determined by subtracting the DTMs generated after each machine pass (DTM1, DTM2, DTM3, DTM4) from the initial DTM (DTM0), captured before operations for all trail configurations.

To evaluate the accuracy of the UAV depth measurements, we compared a total of 198 manual reference points, as described in Section 2.2.1, with the mean DTM value within a 10 cm buffer around each point. Accuracy was assessed separately for each pass and each trail to ensure consistency across different configurations. We then calculated error metrics, including the mean absolute error (MAE) (Eq. (1)), root mean square error (RMSE) (Eq. (2)), relative RMSE (RMSE%) (Eq. (3)), and the standard deviation of differences (SD) (Eq. (4)).

$$\mathrm{MAE} = \frac{1}{n}\sum_{i=1}^{n}|y_i - \hat{y}_i| \tag{1}$$

$$\mathrm{RMSE} = \sqrt{\frac{1}{n}\sum_{i=1}^{n}(y_i - \hat{y}_i)^2} \tag{2}$$

$$\mathrm{RMSE\%} = \left(\frac{\mathrm{RMSE}}{\bar{y}}\right) \times 100 \tag{3}$$

$$\mathrm{SD} = \sqrt{\frac{1}{n-1}\sum_{i=1}^{n}\left[(y_i - \hat{y}_i) - \overline{d}\right]^2} \tag{4}$$

In equations (1)–(4), y_i are the observed (manual) values, $\hat{y}_i$ are the predicted (UAV-derived) values, n is the number of observations, $\bar{y}$ is the mean of the observed values, and $\overline{d}$ is the mean of the differences $(y_i - \hat{y}_i)$. All statistical analyses and visualisations were performed using Python 3.12.

2.3. Tree stump influence and soil properties

2.3.1. Tree stump mapping

This study analysed tree stump positions and processed DTMs before and after each machine pass, along with manual measurements, to assess the influence of tree root systems on rutting. For each parameter described below, a corresponding raster map was created at a 0.03 m resolution, aligned with the DTM for each trail configuration. Wheel ruts in these areas were manually digitised, and all DTMs and other raster layers were clipped using these polygons. Only the pixels within these polygons were used in further analysis, ensuring that we focused specifically on machine-induced rutting effects.

To obtain precise locations, tree stumps within each trail and their configurations were manually identified using orthomosaics. Each orthomosaic was clipped using a 6-meter buffer around the trail centreline to define the mapping area. We assumed a 6-meter buffer was sufficient to capture all relevant stumps that could potentially influence rut formation within the affected soil zone. This area was then manually mapped to identify stump locations. A polygon was then created for each stump to define its boundaries and calculated the diameter by finding the largest distance between its vertices (Eq. (5)).

$$d = \max\left(\sqrt{(x_2 - x_1)^2 + (y_2 - y_1)^2}\right) \tag{5}$$

Eq. (5) defines d as the largest distance between any two vertices, and (x_1, y_1) and (x_2, y_2) as coordinates of any two vertices of the polygon. We also generated centroid points for further impact assessment. The summary of diameters across all sites and trails is presented in Fig. 5.

2.3.2. Peat strength estimation

Peat soils have a highly variable bearing capacity influenced by moisture content. In this study, peat strength refers to the unconfined compressive strength of peat and was estimated based on existing guidelines from plate loading tests, which reflect the unconfined compressive strength of peat under deformation conditions (Miljøministeriet, 2005).

In dry conditions, peat strength typically ranges from 40 to 70 kPa, while in moist conditions, it decreases to between 10 and 40 kPa (Miljøministeriet, 2005). The peat's moisture content on the site averaged 86% (%wgt), ranging from 84% to 89% based on field measurements. To align the peat strength with the specific moisture levels of each trail, we estimated the peat strength (S_{peat}) for each pixel using the following formula:

$$S_{\mathrm{peat}} = 40 - 3 \times (W_{\mathrm{peat}} - 85) \tag{6}$$

where S_{peat} is the estimated peat strength (kPa), and W_{peat} is the peat moisture content ($\%_{\mathrm{wgt}}$). In this formula, the base strength is 40 kPa at a moisture level of 85%. The strength increases to approximately 42 kPa at the lowest recorded moisture level of 84%, while it decreases to approximately 27 kPa at the highest recorded moisture level of 89%.

2.3.3. Distance to the stump

The influence of stumps on soil stability diminishes with distance (Schwarz et al., 2010). To quantify this effect, we used an exponential decay model to represent the cumulative influence of multiple stumps (Fig. 2). While exponential decay models are widely used in environmental and geomechanical studies to describe processes such as root reinforcement decay and soil production (Masi et al., 2021), to our knowledge, they have not yet been applied specifically to understanding the role of stumps in rut formation.

The modelled influence follows an exponential decline, with the effect strongest near the stump and gradually decreasing with distance (Eq. (7)).

$$I(d) = e^{-k \cdot d} \tag{7}$$

where $I(d)$ is the influence at a distance d, d is the distance from the centre of the stump to the centre of the pixel being evaluated in m, and k is the decay constant that controls how quickly the influence diminishes. A higher k value indicates a rapid decline in influence, while a lower k value means the influence extends over a broader area.

We determined the decay constant ($k = 0.3$) by evaluating a range of candidate values ($k = 0.1, 0.2, 0.3, 0.4, 0.5, 1.0$) in an iterative manner. The selected value was chosen to achieve a realistic balance between the influence range and decay rate, ensuring that the influence extends spatially in a reasonable manner without exaggerating its effect.

To determine the distance from the stump to the centre of each pixel d, we used the Euclidean distance equation (Eq. (8)).

$$\mathrm{distance} = \sqrt{(x_{\mathrm{pixel}} - x_{\mathrm{stump}})^2 + (y_{\mathrm{pixel}} - y_{\mathrm{stump}})^2} \tag{8}$$

where, x_{stump} and y_{stump} are the coordinates of the stump's centroid, $x_{\mathrm{pixel}}, y_{\mathrm{pixel}}$ are the coordinates of the centre of each pixel in the raster.

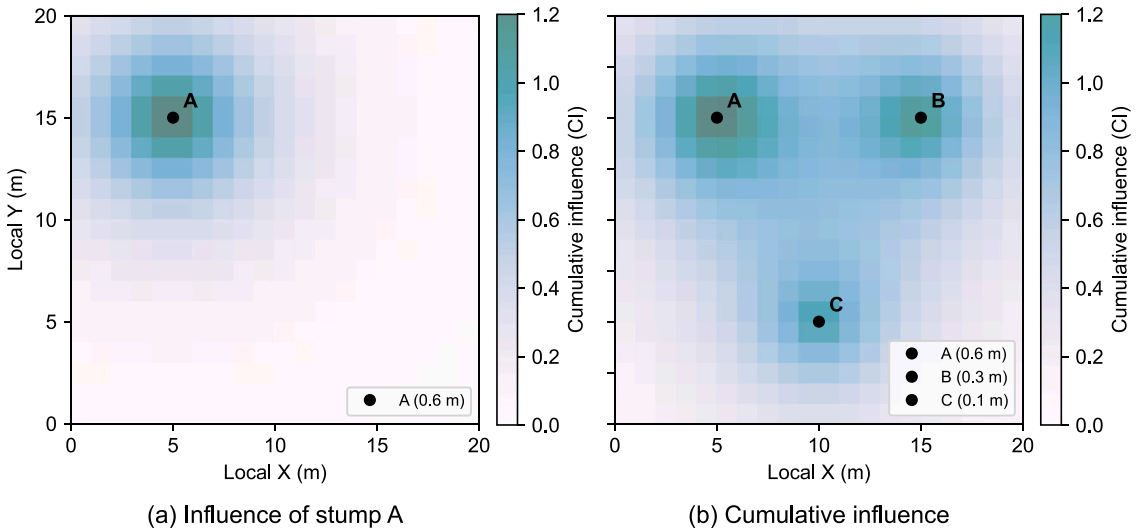

Fig. 2. Visualisation of distance-based stump influence. (a) Influence of a single stump (A) modelled using an exponential decay function. (b) Cumulative influence using the same exponential decay function from multiple nearby stumps (A, B, C).

Given that larger stumps have a more substantial influence due to more extensive root systems, we adjusted the function to include stump diameter as a scaling factor (Eq. (9)).

$$I(d, D) = \left(1 + \alpha \cdot \frac{D}{D_{\text{ave}}}\right) \cdot e^{-k \cdot d} \tag{9}$$

where D is the stump diameter, D_{ave} is the average diameter of all stumps, and α is a scaling constant controlling the effect of stump diameter on influence.

To account for overlapping influences from multiple stumps, the cumulative influence (CI) at each pixel (Fig. 2) was calculated as the sum of the adjusted influences from all nearby stumps (Eq. (10)). This cumulative effect aims to replicate actual environmental conditions, where multiple tree root systems often interact, creating an interlinked network that improves soil stability (Schwarz et al., 2016).

$$CI = \sum_{\text{stumps}} I(d, D) \tag{10}$$

In Eq. (10), $I(d, D)$ is the influence of an individual stump at a distance d from the pixel, scaled by the stump's diameter D. CI represents the cumulative influence at each pixel, calculated by summing contributions from all stumps. Stumps with $D > D_{\text{ave}}$ have a scaling factor greater than 1, increasing their influence, those with $D < D_{\text{ave}}$ have a scaling factor less than 1, reducing it. This summation accounts for overlapping root systems and their combined effects.

2.3.4. Root reinforcement modelling

To estimate root reinforcement in our study, we used a simplified interpolation and curve-fitting method based on the findings of Schwarz et al. (2010). The study reported maximum reinforcement values for Norway spruce (*Picea abies*) at specific distances from the tree trunk, grouped by stump diameters of 20, 40, and 60 cm. We expanded on this data by interpolating reinforcement values at 50 cm intervals. Using the interpolated values, we applied a reverse sigmoidal function (Eq. (11)) to create smooth curves for each stump diameter group. The reverse sigmoidal function, in this case, captures the natural decline of root support, being most robust near the stump and gradually declining outward. This resulted in specific equations for each group (Eq. (11), Table 1). The general function is defined as:

$$RRV(x) = \frac{L}{1 + e^{-k(x - x_0)}} \tag{11}$$

where RRV is the root reinforcement value (kPa) at a given distance x from the stump, where x is measured in m. L is the maximum reinforcement level derived from the data (kPa), k controls the steepness of the curve, x_0 is the distance at which the curve has an inflection point, x is the distance from the stump to the pixel being evaluated.

Table 1
Logistic curve coefficients for different stump diameters.

Diameter class (cm)	L (kPa)	k	x_0
20	21.09	−1.006	2.61
40	45.16	−1.046	3.74
60	79.55	−1.016	4.01

These coefficients were then applied iteratively to each digitised stump across the study area, considering the stump diameter, the distance from the stump centre to the centre of each pixel (Eq. (8)), and the coordinates of each pixel.

Specific parameters (Table 1) were used to compute the reinforcement value for each pixel based on its distance from the stump, following a sigmoidal decay curve. The influence radius was guided by the approach described in Schwarz et al. (2010), which relates stump diameter to the extent of root reinforcement, with distances indicating where reinforcement approaches zero ($RRV = 0$). For areas where the reinforcement effect of multiple stumps overlapped, we summed the reinforcement values to account for the combined effect. This was done by iterating over each stump, applying the logistic function within its influence radius, and accumulating the values in an RRV raster. The resulting RRV raster values were then normalised to a scale of 0–100 using Eq. (12), resulting in a root reinforcement map that reflects the combined spatial influence of all stumps across the study area.

$$R_{\text{norm}} = 100 \cdot \frac{R_{\text{final}} - R_{\text{min}}}{R_{\text{max}} - R_{\text{min}}} \tag{12}$$

where R_{final} represents the summed reinforcement values, and R_{min} and R_{max} are the minimum and maximum reinforcement values across the study area.

2.4. Statistical analysis

To evaluate how tree stumps influence rut depth, we categorised CI values within each trail and configuration into five groups: "very high", "high", "moderate", "moderately low", and "low". Areas classified as "very high" contained dense, large stumps, contributing to a strong influence, while "low" areas had fewer stumps and less influence. The categorisation was based on the distribution of the CI values,

Table 2
Effect size (ε^2) interpretation thresholds for the Kruskal–Wallis test.

Effect size	Threshold (ε^2)
Small	$\varepsilon^2 \geq 0.01$ and < 0.06
Medium	$\varepsilon^2 \geq 0.06$ and < 0.14
Large	$\varepsilon^2 \geq 0.14$

which were split into these groups according to natural breaks observed in the histogram and Kernel Density Estimation (KDE) plots. These breakpoints were chosen to represent shifts in the data, ensuring each group captured a distinct range of influence.

The data were first tested for normality using the Shapiro–Wilk test across straight and curved configurations. Since the results indicated a non-normal distribution, we used the Kruskal–Wallis test to assess whether rut depth significantly differed among distance groups within each pass and trail configuration. If $p < 0.05$, then at least one distance group had a significantly different rut depth. If $p > 0.05$, we concluded that rut depth did not significantly vary across distance groups within that configuration. Due to the large and uneven sample sizes among distance groups, we employed balanced random subsampling to ensure fair statistical comparisons and to mitigate the risks associated with large-sample biases. To additionally assess the stability of our samples, we repeated the Kruskal–Wallis test across five independent iterations, each using a new random subsample from the dataset.

To determine the effect size of rut depth variations, we computed epsilon-squared (ε^2) (Eq. (13)) as a measure of effect size for the Kruskal–Wallis test. This metric helps determine the proportion of variance in rut depth explained by distance groups, with values above 0.06 indicating a moderate effect and values above 0.14 (Table 2) suggesting a strong influence of stump presence on rut depth formation (Carroll & Nordholm, 1975; Glass & Hakstian, 1969).

$$\varepsilon^2 = \frac{H}{\frac{N^2-1}{N+1}} \tag{13}$$

where, H is the Kruskal–Wallis test statistic, and N is the total number of observations.

A small effect size might suggest a significant but weak influence of stump proximity on rut depth, while a large effect size would indicate that stump proximity has a much stronger influence on rut formation.

2.5. ML for depth prediction

To evaluate how well rut depth can be predicted using soil properties, stump influence, and environmental factors, we implemented a Random Forest (RF) model. Machine learning algorithms identify complex spatial and non-linear relationships between inputs and targets that traditional statistical methods often fail to capture. For instance, RF constructs multiple decision trees and combines their outputs for more reliable predictions (Breiman, 2001). We employed an RF model to predict rut depth based on soil properties, the presence of stumps, and other factors. The model used only pixels where the DTM-derived depth value was below 0 as the dependent variable (Y), while soil, environmental, and machine parameters served as independent variables (X) (Table 3).

The selection of RF was based on the distribution of the data and the complexity of the predictor variables. Kolmogorov–Smirnov tests and skewness analysis indicated that key variables (CI, RRV, and SM) were highly skewed, rejecting the normality assumption required for linear regression. Additionally, RRV and CI follow logistic and exponential decay functions, both of which introduce non-linearity and interaction effects.

The model was trained separately for each pass over various datasets, including (a) the full or combined dataset as well as separate datasets for (b) straight and (c) curved trails. We tuned the RF hyperparameters to improve model accuracy using RandomizedSearchCV (Pedregosa et al., 2011). The final configuration used was $n_{\text{estimators}} = 200$, $max_{\text{depth}} = \text{None}$, $min_{\text{samples\_split}} = 5$, and $min_{\text{samples\_leaf}} = 1$.

Table 3
List of dependent (Y) and independent (X) variables used in the Random Forest (RF) models.

Variable ID	Variable	Units
Y	Rut depth (RD)	m
X_1	Root reinforcement value (RRV)	arbitrary units
X_2	Cumulative distance from the stump (CI)	arbitrary units
X_3	Moisture-dependent peat strength (S_{peat})	kPa
X_4	Shear modulus (G_{trail})	kPa
X_5	Maximum NGP (NGP_{max})	kPa
X_6	Mean NGP (NGP_{mean})	kPa

Feature importance scores were initially determined using the RF model, after which Recursive Feature Elimination (RFE) was utilised to refine the model for both straight and curved trail configurations, as well as for the combined dataset. This process iteratively removes the least essential features while maintaining predictive performance, and the final model retained the top three features ranked by importance. Separate RF models were then trained for each configuration and pass.

Model performance was evaluated using 10-fold cross-validation for each configuration and pass, where the dataset was randomly divided into 10 equal-sized folds. The process was repeated 10 times. In each iteration, one fold was used as the test set while the remaining nine folds were used for training. This ensured that every data point was used once for testing and nine times for training. Predictive accuracy was quantified using the coefficient of determination (R^2) (Eq. (14)), and model performance results are reported as the average R^2 values obtained across the 10 cross-validation folds.

$$R^2 = 1 - \frac{\sum_{i=1}^{n} \left(y_i - \hat{y}_i\right)^2}{\sum_{i=1}^{n} \left(y_i - \bar{y}\right)^2} \tag{14}$$

where, R^2 is the coefficient of determination, n is the number of data points, y_i is the actual value of the ith data point, $\hat{y}_i$ is the predicted value of the ith data point; $\bar{y}$ is the mean of the actual values ($\bar{y} = \frac{1}{n}\sum_{i=1}^{n} y_i$), $\sum_{i=1}^{n} \left(y_i - \hat{y}_i\right)^2$ is the residual sum of squares (SSR), $\sum_{i=1}^{n} \left(y_i - \bar{y}\right)^2$ is the total sum of squares (SST).

To demonstrate the model's performance, we applied the best-performing RF configuration to a synthetic spatial dataset consisting of simulated shear modulus values and randomised tree stump distributions. Shear modulus values were generated by randomly placing control points across the area and interpolating them over a grid using cubic interpolation to create a continuous surface. Tree stumps were also randomly distributed, with diameters ranging from 10 to 40 cm and a minimum spacing of 2 m between them (60 stumps in total). To simulate more natural clustering, each stump's diameter was averaged with those of nearby stumps. The key predictor variables identified in the model analysis were used to generate corresponding pixel-wise input datasets. The trained model was then applied to this synthetic area, and the predictions were visualised as a contour map. The input raster grid resolution was initially set to 0.03 m and later resampled to 0.5×0.5 m for visualisation purposes.

3. Results

3.1. Rut depth analysis

The average rut depth across all trails and configurations was 15.5 cm for manual measurements and 12.5 cm for UAV measurements, with standard deviations of 7.6 cm and 8.3 cm, respectively. Both

Table 4
Summary statistics of manual and UAV measurements across machine passes. Each value represents the overall statistic, with values in parentheses indicating the straight (first) and curved (second) configurations.

	Mean (manual)	Mean (UAV)	SD (manual)	SD (UAV)	MAE (cm)	RMSE (cm)	RMSE (%)
Pass 1	11.1 (11.3, 10.7)	10.6 (10.9, 9.9)	5.9 (6.4, 4.8)	5.3 (5.9, 4.0)	2.2 (1.8, 2.8)	3.0 (2.4, 3.6)	26.5 (21.4, 34.1)
Pass 2	15.0 (14.9, 15.1)	14.1 (13.5, 15.0)	6.6 (7.2, 5.5)	6.0 (6.4, 5.0)	2.3 (2.0, 2.7)	3.1 (2.6, 3.8)	20.8 (17.5, 25.3)
Pass 3	19.3 (19.2, 19.5)	17.6 (17.6, 17.7)	7.3 (7.8, 6.3)	7.0 (7.7, 5.7)	2.7 (2.4, 3.1)	3.5 (3.0, 4.2)	18.3 (15.9, 21.8)
Pass 4	20.5 (20.6, 20.2)	19.8 (19.8, 19.9)	7.6 (8.1, 6.6)	6.8 (6.9, 6.7)	3.3 (2.7, 4.2)	4.2 (3.4, 5.2)	20.3 (16.5, 25.7)
Total	15.5	12.5	7.6	8.3	2.5	3.3	24.9

datasets showed variation in rut depth across trails and configurations, with differences influenced by the number of passes (Table 4).

For manual measurements, rut depth ranged from –8 cm (N = 4) to a maximum of 41 cm, with negative values occurring due to upwelling or measurement difficulties near stumps. UAV measurements followed a similar trend but ranged from 0 cm to 40 cm, showing slightly lower values for deeper ruts, particularly on curved trails (Fig. 3). Across passes, UAV consistently measured lower rut depths than manual measurements. In Pass 1, UAV underestimated by 0.5 cm (10.6 cm vs. 11.1 cm), with the gap increasing slightly in later passes. In Pass 4, UAV measured 19.8 cm compared to 20.5 cm manually, maintaining a consistent underestimation trend. Measurement variability also increased as ruts deepened. SD remained similar in early passes (5.9 cm manual and 5.3 cm UAV in Pass 1) but showed a slight decrease in UAV measurements in later passes (7.6 cm manual and 6.8 cm UAV in Pass 4). The UAV underestimation was more consistent in straight trails, but greater variability was observed in curved trails, where SD reached 8.1 cm for manual measurements in Pass 4 compared to 6.7 cm for UAV.

Rut depth increased from Pass 1 to Pass 4, as expected, with each pass further compacting the soil and increasing rut formation. This effect was more pronounced on curved trails, where lateral forces exerted by the machine contributed to deeper ruts by both compacting and displacing the soil. These trends were consistent with findings in the same study area (Ala-Ilomäki et al., 2021). The boxplots in Fig. 3 illustrate this pattern, showing that straight trails exhibited lower rut depths than curved trails in both manual (Fig. 3(a)) and UAV-derived (Fig. 3(b)) measurements.

While both methods captured the overall trend of rut formation, differences in accuracy were observed. Manual measurements (Fig. 3(a)) showed a broader distribution of rut depths, particularly in the earlier passes, while UAV measurements (Fig. 3(b)) followed a similar pattern but with consistently lower values.

Measurement errors increased as passes progressed. The MAE increased from 2.2 cm in Pass 1 to 3.3 cm in Pass 4, while RMSE increased from 3.0 cm to 4.2 cm (Fig. 4). RMSE was highest in curved trails, reaching 5.2 cm in Pass 4 compared to 3.4 cm in straight trails, highlighting the UAV's difficulty in capturing the full depth of irregular ruts. SD for both manual and UAV measurements increased with each pass, showing greater variability in rut formation as deeper ruts developed due to soil displacement and compaction. Several outliers (> 30 cm) were recorded, primarily in curved trails, where machine-induced lateral displacement resulted in more uneven rut profiles.

3.2. Tree stump influence and soil properties

Tree stump diameters ranged from 5.4 cm to 30.0 cm, with fewer stumps at the extreme ends of this range. The average diameter was 22.5 cm, with a standard deviation of 8.1 cm, indicating moderate variation. In total, 269 stumps were analysed. Fig. 5 shows the distribution of stump diameters across different trails and configurations with consistent median values. No significant differences were observed between straight and curved trail configurations, and the overall average diameter remained stable across all trails.

Peat moisture content averaged 86% across all trails, ranging from 84% to 89%, with higher moisture levels observed on curved trails. The estimated peat strength (Table 5) varied accordingly, ranging from 35.0 to 42.6 kPa on straight trails and 27.0 to 37.7 kPa on curves, indicating weaker soil conditions and higher susceptibility to rutting in curved sections. The shear modulus of the peatland top layer exhibited significant variability, with values ranging from 30.8 to 383.4 kPa on straight trails, while curved trails showed considerably lower stiffness, ranging from 23.9 to 138.3 kPa (Table 5).

To illustrate how stump presence and terrain changes interact spatially, Fig. 6 presents UAV-derived elevation differences (a–c), calculated as the difference between the post-pass DTM and the pre-operation DTM, alongside the cumulative stump influence map (d) for one representative straight trail. Areas with higher cumulative influence, typically near larger or clustered stumps, tend to align with zones of reduced rutting, suggesting a local stabilising effect.

Statistical analysis

To assess how stump presence influenced rut formation, rut depth values were analysed across the five CI groups (very high, high, moderate, mod-low, and low) (Table 6). The Shapiro–Wilk test indicated a non-normal distribution for both straight ($W = 0.97$, $p < .05$) and curved ($W = 0.93$, $p < .05$) configurations. Therefore, the Kruskal–Wallis test was performed to compare the rut depth across influence groups. Results showed significant differences in rut depth among influence groups across all passes and configurations ($p < 0.05$) (Table 7). To ensure fair statistical comparisons and mitigate biases from uneven sample sizes, balanced random subsampling ($n = 5000$ per group) was applied. The Kruskal–Wallis test was repeated across five independent iterations using different random subsamples, confirming that results remained stable. These results are presented in Table 7.

The H-statistic from the Kruskal–Wallis test measures rank-based differences between groups, with higher H-values indicating stronger differences among the CI groups. For straight trails, the H-statistics ranged from 94.61 (Pass 1) to 280.79 (Pass 4), with Pass 4 showing the highest value, indicating stronger differences between the groups. This suggests that, during Pass 4, rut depth varied significantly, with areas of high stump density showing deeper ruts compared to areas further from stumps. For curved trails, the H-statistics ranged from 74.71 (Pass 1) to 524.38 (Pass 4), with similarly significant differences in rut depth across influence groups, especially in Pass 4. This indicates that the presence of stumps impacts rut depth across both trail types, but the influence appears to be stronger in curved trail sections, possibly due to differences in the terrain.

The epsilon-squared values indicate that stump presence has a moderate to large effect on rut depth in curved trails, with medium effects observed in straight trails, especially in Pass 4. For straight trails, the ε^2 values ranged from 0.04 to 0.20, indicating a small to medium

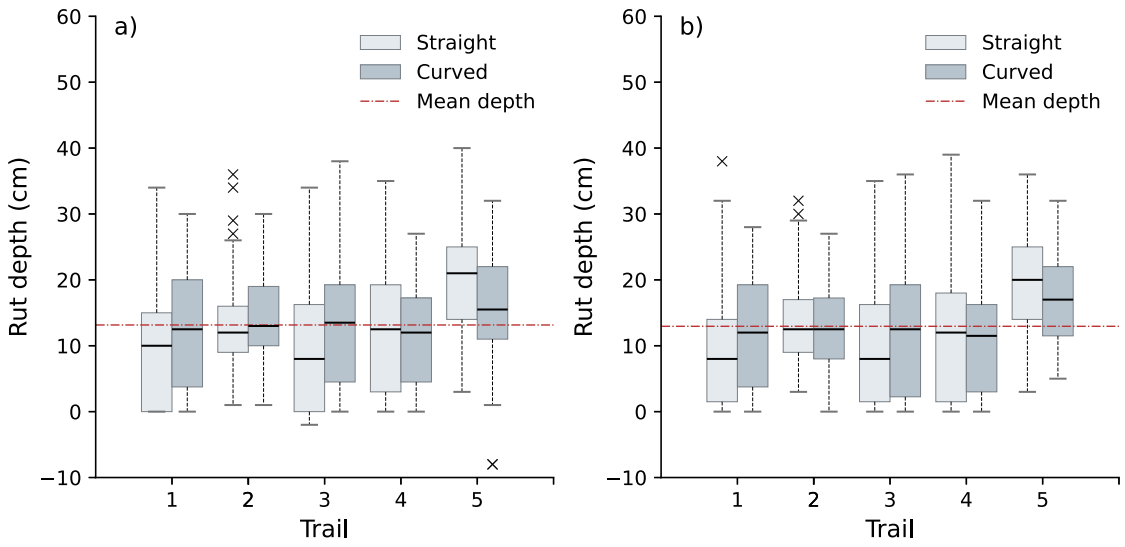

Fig. 3. Descriptive statistics of manual and UAV rut depth measurements. (a) Boxplot of manual rut depth measurements by trail type (straight and curved). The box shows the 1st (25%) and 3rd (75%) quartiles, while the whiskers represent data within 1.5 times the interquartile range (IQR). The red dashed line represents the mean rut depth of 13.2 cm across all manual measurements. (b) Boxplot of UAV rut depth measurements by trail type (straight and curved). The same style as (c), with the red dashed line representing the mean rut depth for UAV measurements of 12.9 cm across all UAV measurements. (For interpretation of the references to colour in this figure legend, the reader is referred to the web version of this article.)

Table 5
Summary of peat moisture, peat strength, and shear modulus by configuration.

Configuration	Peat moisture (%)			Peat strength (kPa)			Shear modulus (kPa)		
	Min	Max	Mean	Min	Max	Mean	Min	Max	Mean
Straight	84.1	86.7	85.2	35.0	42.6	39.3	35.2	383.4	86.3
Curved	85.7	89.3	87.0	27.0	37.8	34.0	23.9	138.3	51.8

Table 6
Summary statistics of rut depth, including median, mean, and standard deviation (SD), all expressed in centimeters (cm), by cumulative influence (CI) groups and configurations.

Influence group	Configuration	Median (cm)	Mean (cm)	SD (cm)
Low	Straight	14	15	9
Low	Curved	18	19	11
Mod-low	Straight	14	15	9
Mod-low	Curved	16	18	11
Moderate	Straight	14	15	8
Moderate	Curved	14	15	10
High	Straight	13	14	8
High	Curved	12	13	9
Very high	Straight	9	12	9
Very high	Curved	9	10	8

Table 7
Kruskal–Wallis test for depth variations among cumulative influence (CI) groups by trail configuration and pass. The Epsilon-squared (ϵ^2) column is highlighted to reflect the corresponding effect strength with light grey for small, light blue for medium, and a deeper blue for large effects, as defined in Table 2.

Configuration	**Pass**	**H-statistic**	**p-value**	**Epsilon-squared (ϵ^2)**
Straight	1	94.61	< 0.05	0.06
Straight	2	219.01	< 0.05	0.07
Straight	3	119.24	< 0.05	0.04
Straight	4	280.79	< 0.05	0.20
Curved	1	74.71	< 0.05	0.02
Curved	2	397.23	< 0.05	0.10
Curved	3	334.86	< 0.05	0.09
Curved	4	524.38	< 0.05	0.32
Total	All	**1701.27**	**< 0.05**	**0.07**

effect size. Pass 4 had the highest effect size (ϵ^2 = 0.20), suggesting that the influence of stumps on rut depth was most pronounced in this pass. For curved trails, the ϵ^2 values ranged from 0.02 to 0.32, showing a similar pattern. Pass 4 again had the highest effect size (ϵ^2 = 0.32), which is considered a medium to large effect, indicating a strong impact of stump presence on rut formation in curved trails.

The results are further visualised in Fig. 7, which presents boxplots of rut depth across influence groups for each pass and configuration. The plots illustrate a consistent trend where rut depth tends to be lowest in areas of high stump presence (very high CI) and increases as the distance from stumps increases (low CI).

3.3. ML for depth prediction

After training the model to predict rut depth, the RF models identified and ranked the most influential predictor variables. The results show that cumulative stump influence, root reinforcement value, and shear modulus were the top three predictors across all trail configurations (combined, straight, and curved datasets). These features were consistently ranked highest by the RF model and selected by RFE. In contrast, moisture-dependent peat strength, along with mean and maximum NGP, had minimal contribution across all configurations (Fig. 8).

A detailed analysis of feature significance across various trail setups shows distinct patterns. In the combined dataset (Fig. 8(a)), RRV (0.394) and CI (0.384) contributed almost equally to rut depth prediction, with RRV slightly outperforming CI. G_{trail} was the third most important feature but had a much lower score (0.109), indicating a weaker influence. For straight trails (Fig. 8(b)), RRV (0.429) and CI (0.419) recorded their highest importance scores, reinforcing their dominant role in rut formation. In contrast, G_{trail} had minimal influence (0.094), while the remaining features had negligible impact. In curved trails (Fig. 8(c)), RRV remained the most influential predictor (0.421), but CI's importance slightly declined (0.358). Interestingly, G_{trail} played a greater role (0.146), suggesting that variations in shear modulus may

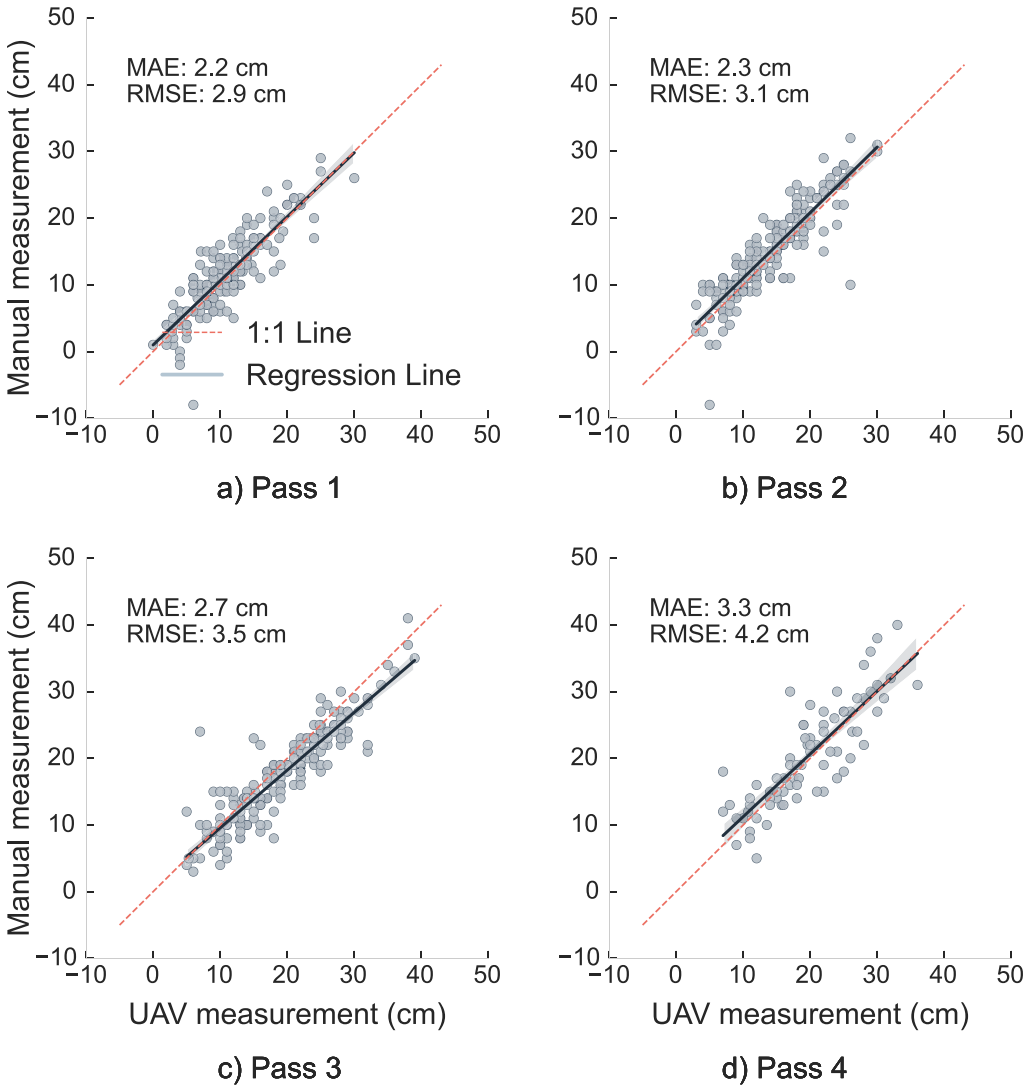

Fig. 4. Scatterplot of manual and UAV measurements for Pass 1 to 4 (a–d). The blue line represents the regression line, while the red dashed line indicates the 1:1 reference line. The Mean Absolute Error (MAE) and Root Mean Square Error (RMSE) are provided in cm for each pass. (For interpretation of the references to colour in this figure legend, the reader is referred to the web version of this article.)

be more influential in curved terrain, where soil resistance dynamics are likely to differ from those in straight trails.

It is important to note that both RRV and CI were derived using similar approaches, as both incorporate stump diameter and distance to the stump as key input elements. Due to their conceptual similarities, they demonstrated a strong correlation of $R^2 = 0.76$. However, they capture different aspects of stump-root influence on soil stability. Therefore, both were retained for further model training, as feature importance analysis consistently ranked them among the top predictors across all setups. In fact, model performance tests showed that removing CI led to a 78.6% reduction in predictive accuracy, while removing RRV caused an 80.8% reduction, highlighting their contribution to model performance. RF performs best when it can use non-linear relationships and interactions between features. Removing one feature restricts the model's capacity to detect threshold effects in RRV, which indicate root strength, and to account for distance decay effects in CI, where influence decreases with distance. This means that features provide important information to the model. Therefore, RRV, CI, and G_{trail} were used for further model training (Fig. 8).

The dominance of RRV and CI across all configurations suggests that stump presence plays an essential role in soil stability and rut formation. The stronger influence of G_{trail} in curved trails implies that shear modulus variations have a greater effect on rut formation when the machine path is nonlinear. The negligible impact of peat strength, NGP_{mean}, and NGP_{max} suggests that nominal ground pressure alone may not sufficiently explain rut formation, reinforcing the need to include root-related features for more accurate predictions.

To further validate the RF model, 10-fold cross-validation was performed across different configurations (Fig. 9), and the results are summarised in Table 8. The model demonstrated high predictive capability, with average training R^2 values consistently above 0.96 across all configurations, and test R^2 values varying by trail type. In the combined dataset, test R^2 ranged from 0.73–0.85, indicating good generalisation across trail types. In straight trails, lower test R^2 values (0.69–0.77) suggest weaker predictive performance for rut depth, whereas curved trails achieved the highest test R^2 values (0.75–0.85), indicating better accuracy under these conditions (Fig. 9).

The lower R^2 values in straight trails may be due to repeated passes over the same track, which progressively compacts the soil and makes rut formation less sensitive to individual predictor variables. In contrast, curved paths show more significant variability due to uneven soil compaction and lateral displacement pressures. On curved trails, the turning motion of the steel trails can induce lateral displacement and localised shear stresses in the soil, particularly when differential lock is engaged. This creates uneven loading and increased soil

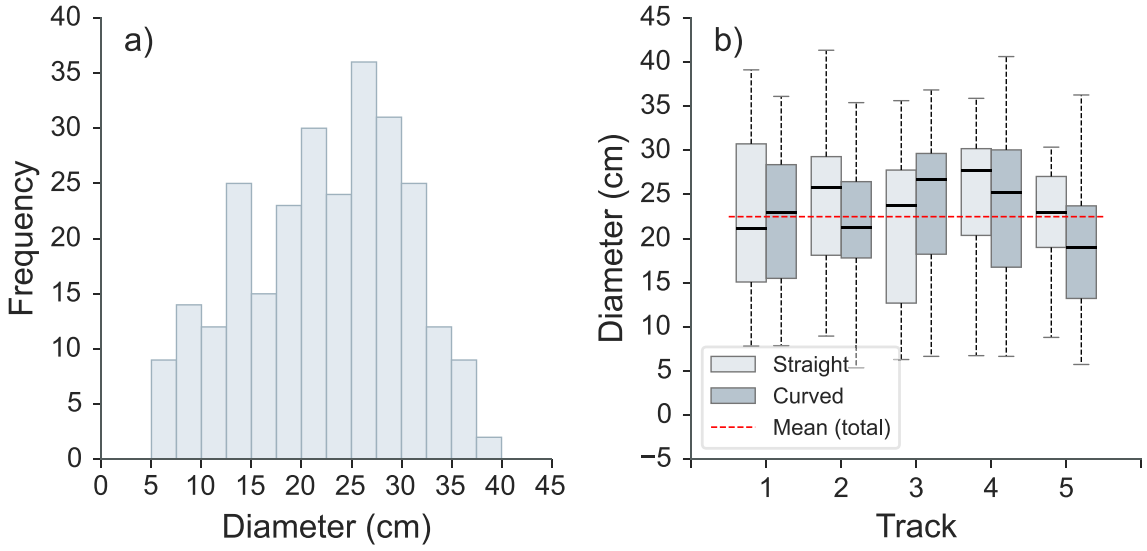

Fig. 5. Descriptive statistics of tree stump diameters (cm) from digitised polygons. The histogram (a) shows the diameter distribution in cm. The boxplot (b) displays average diameters by trail and configuration (straight or curved), with boxes representing the interquartile range (IQR) and whiskers covering 95% of the data. The line inside each box is the median, and the red dashed line indicates the overall mean diameter. (For interpretation of the references to colour in this figure legend, the reader is referred to the web version of this article.)

Table 8
Random forest results presented as average performance metrics from 10-fold cross-validation by configuration and pass, with training and testing dataset sizes indicated in thousands of pixels (Kpx).

Configuration	Pass	Train size (Kpx)	Test size (Kpx)	R^2 (Train)	R^2 (Test)
Straight	1	160.50	40.10	0.96	0.69
	2	160.60	40.10	0.96	0.74
	3	172.70	43.10	0.97	0.77
	4	74.20	18.50	0.96	0.74
Curved	1	238.60	59.60	0.96	0.75
	2	226.90	56.70	0.97	0.81
	3	200.60	50.10	0.98	0.85
	4	84.30	21.10	0.97	0.82
Combined	1	399.10	99.70	0.96	0.73
	2	387.50	96.80	0.97	0.80
	3	373.30	93.30	0.98	0.83
	4	158.60	39.60	0.97	0.79

deformation, contributing to greater variability in rut development, which the model captures more effectively. Additionally, the higher importance of G_{trail} in curved trails suggests that soil resistance plays a more significant role in non-linear machine routes. The relationship between vehicle dynamics and soil characteristics is more complex in curved configurations, resulting in stronger correlations between G_{trail} and rut development than in straight paths.

The RF model trained on observed rut depths was then applied to a synthetic spatial dataset composed of randomly distributed stumps and a simulated shear modulus map. The results showed that areas with smaller stumps generally had deeper predicted rut depths, while areas with larger and denser stumps showed shallower predicted depths (closer to 0 cm) across all three passes (Fig. 10(a)–(c)). This pattern also aligns with the model's feature importance results, where RRV and CI were identified as the most influential predictors (Fig. 8). Larger stumps likely indicate stronger and broader root systems, which help stabilise the soil and reduce deformation. Predicted rut depth also increased progressively with each machine pass, especially in areas with fewer stumps and lower shear strength. While the results are based on synthetic input data, they demonstrate how spatially explicit rut depth modelling can support forest operations planning. By identifying areas at greater risk of soil disturbance, managers can optimise machine routes, minimise long-term impacts, and support more sustainable harvesting practices.

4. Discussion

This study investigated the role of tree stumps in rut formation on peatland soils, combining UAV-based and manual rut depth measurements, statistical analysis, spatial modelling, and machine learning techniques. The findings confirm that stump presence contributes to soil stability and mitigates machine-induced deformation. Rut depths were shallower near stumps, with the influence gradually weakening with distance. The impact of stumps was most significant in curved trails, where lateral soil displacement was greater, with effect sizes ranging from small to large (ε^2 = 0.02–0.32). Stump-related variables (CI and RRV) and shear modulus (SM) were among the strongest predictors of rut depth. Machine learning models incorporating stump effects demonstrated strong predictive accuracy (R^2 = 0.69–0.85) in both straight and curved trails. These findings underscore the importance of considering stump presence in forest operations to improve machine path planning and support sustainable management. When used alongside DTW maps, these models could improve decision-making, minimise soil disturbance and reduce the environmental footprint of forestry activities.

The study first compared UAV-based and manual rut depth measurements to assess the correspondence between the two methods. UAV-derived data provided consistent, high-resolution information and captured the same rut formation trends as manual measurements. Slightly lower values were observed in deeper ruts, particularly in curved trails and later passes, with average differences around 3 cm and maximum deviations of 3.3 cm. These differences likely reflect how each method interacts with the terrain more than inherent measurement inaccuracies. UAV-derived rut depths were extracted by averaging digital terrain model (DTM) values within a 10 cm area around each manual point, which may smooth out localised extremes. Moreover, photogrammetric models often define the ground surface at the top of low vegetation, such as moss and blueberry shrubs, while manual measurements are taken directly at the peat surface, potentially penetrating slightly into the soft, saturated peat, especially under wet conditions. This difference in reference level and surface interaction likely contributes to the observed discrepancies. Other contributing

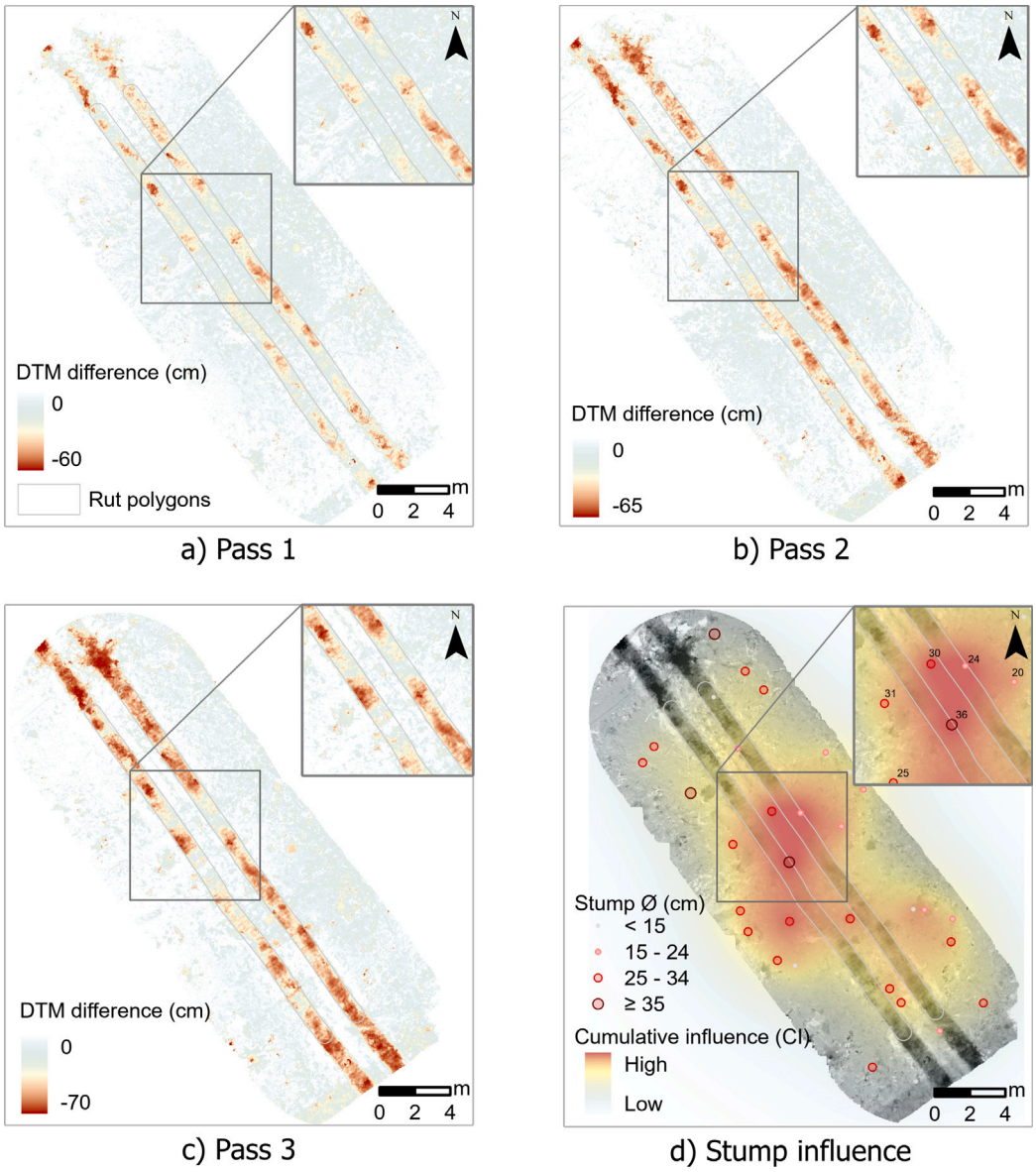

Fig. 6. Elevation change maps derived from UAV-based digital terrain models (DTMs) for one experimental trail (straight configuration). Panels (a–c) show elevation differences after Passes 1, 2, and 3, respectively, calculated as DTM after each pass minus the initial pre-operation DTM. Panel (d) shows the cumulative stump influence (CI), computed from stump diameters and proximity using the methodology described above.

factors may include minor georeferencing offsets, interpolation limitations, and post-processing smoothing in photogrammetry software. In straight trails, where rut formation was more uniform, UAV and manual measurements showed closer agreement. The higher RMSE (3.3 cm) and RMSE% (24.9%) observed in curved trails likely reflect a combination of these methodological factors and do not necessarily imply a systematic UAV bias.

Statistical analysis confirmed that cumulative stump influence significantly affected rut depth, with a small to medium effect in straight trails (ε^2 = 0.04–0.20) and a moderate to large effect in curved trails (ε^2 = 0.02–0.32). The stronger impact in curved trails is likely due to machines not only pressing down but also pushing soil sideways, causing greater soil displacement and deeper ruts. In these conditions, stumps can help stabilise the soil, possibly preventing excessive movement and reducing rut depth. In straight trails, the effect of stumps was smaller but still significant, as rut formation was primarily driven by vertical compression with less influence from lateral soil shifting.

This aligns with the feature importance scores and RFE analysis from the RF model, which identified stump-related variables (CI, RRV) and SM as the most influential predictors of rut depth. In contrast, NGP and peat strength did not significantly influence model performance. While these factors are generally important for rut formation, they were treated as site-specific constants, limiting their relevance to actual conditions. The varying ε^2 values could also be explained by the way CI and RRV were modelled. These variables assume a uniform reduction in stump influence with distance, while rut depth follows a different pattern, usually shallowest near the edges and deepest at the centre. When a stump is located to the side of a rut, CI and RRV decrease steadily, but rut depth first decreases toward the middle and then increases again. This inconsistency likely contributed to the lower effect sizes observed in some passes.

Another consideration is how the machine's weight distribution influences rut depth between the left and right wheel paths. Although left and right rut depths were measured separately, our model treated rutting as a combined process, modelled as a function of distance to the stumps. In reality, wheels may sink unevenly, especially when one side passes over a stump, leading to asymmetric weight distribution and rut formation. When a stump lies directly in the wheel path, it

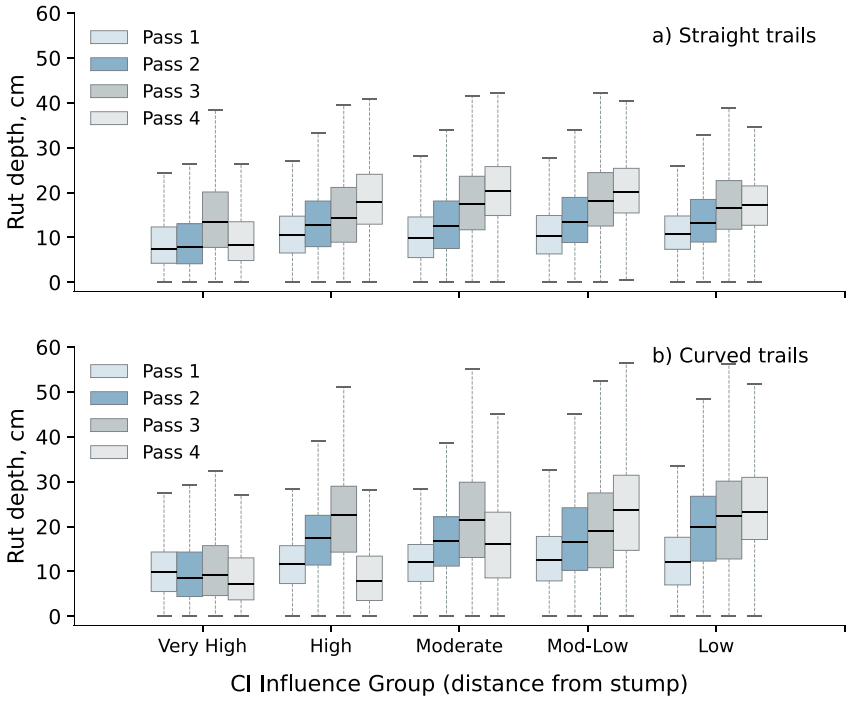

Fig. 7. Boxplots showing rut depth (in cm) distribution across CI influence groups for each pass and trail configuration. The upper plot represents the straight trail.

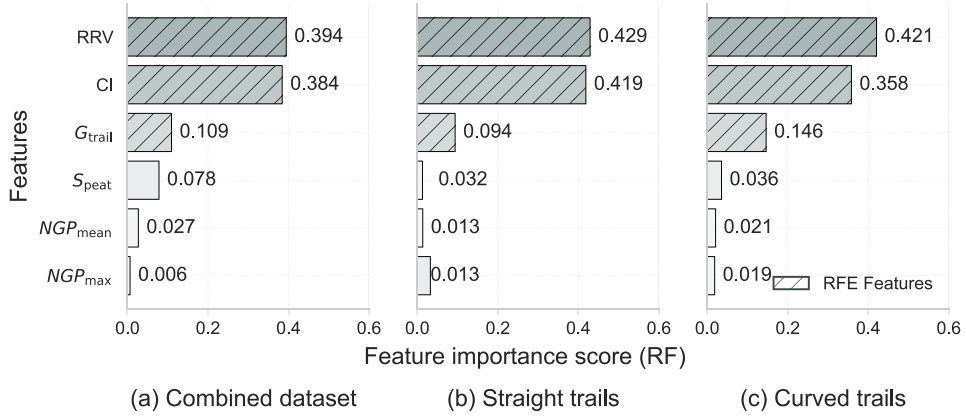

Fig. 8. Feature importance results using the Random Forest (RF) model, where the analysed features are CI (cumulative influence of the stump based on distance from the stump), RRV (root reinforcement value), G_{trail} (shear modulus in kPa), S_{peat} (moisture-dependent peat strength), NGP (mean nominal ground pressure from front and rear in kPa), and Max NGP (maximum nominal ground pressure in kPa). The graph is divided by trail configuration into three categories: combined, straight, and curved, with the line pattern indicating the three most important features identified through Recursive Feature Elimination (RFE).

acts as an obstacle that the machine must climb over, often causing deeper ruts just before and after the stump due to increased resistance to motion and slippage. Meanwhile, the opposite wheel is subjected to an increased wheel load, further contributing to the asymmetry of rut depth. Future studies could explore this by incorporating left and right rut depth averaging or a weight distribution model.

The RF models achieved high predictive accuracy (R^2 = 0.69–0.85), performing better in curved trails than in straight trails. This was unexpected as straight trails were assumed to have more predictable rut patterns. However, the consistent rutting in straight trails made it harder for the model to detect subtle variations. In contrast, the greater variability in curved trails, likely due to lateral soil displacement, provided more diverse data for training, improving model performance. The results of the model application on the synthetic dataset showed that predicted rut depth was generally shallower in areas with larger stumps and higher root reinforcement (Fig. 10). Rut depth increased with each simulated machine pass, especially in zones with fewer or smaller stumps. However, the pattern was not always consistent. Some areas with dense or larger stumps still showed deeper predicted rutting. This highlights the importance of how input parameters like RRV and CI are calculated and suggests that further refinement and customisation of these variables are needed. Nevertheless, these types of spatial predictions could potentially support forest planning by helping to identify high-risk areas, optimise machine routing, and reduce long-term site disturbance.

Prior studies Nevalainen et al. (2017), Roberts et al. (2020) on UAV-based rut depth measurements have demonstrated the effectiveness of aerial photogrammetry in detecting soil deformations. However, they have also noted a slight underestimation of deeper ruts in complex terrain conditions (Marra et al., 2021). Studies on machine-induced rutting emphasise the role of equipment design and soil properties in determining rut depth. Forwarder configuration, bogie tracks, and soil

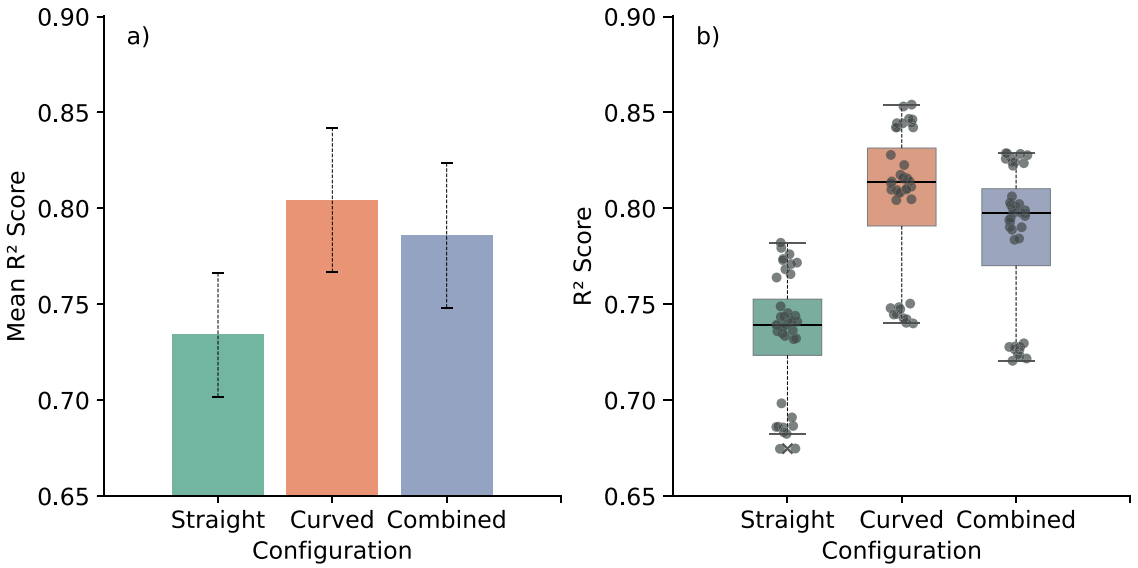

Fig. 9. Random Forest model validation performance across configurations using 10-fold cross-validation, illustrating the R^2 scores obtained for different configurations (straight, curved, combined). (a) displays the mean R^2 scores for each configuration, with error bars representing one standard deviation. (b) Combines a boxplot and swarmplot to visualise the distribution of individual R^2 scores across all folds. The boxplot highlights key statistical measures, including the interquartile range (IQR), whiskers covering 95% of the data, and the median indicated by a solid black line. (For interpretation of the references to colour in this figure legend, the reader is referred to the web version of this article.)

shear strength significantly affect rut formation, with heavier machines and wet conditions leading to deeper ruts (Ala-Ilomäki et al., 2011, 2021). While these studies highlight the influence of machine and soil parameters (Uusitalo & Ala-Ilomäki, 2013), they often overlook stump-root systems as a natural mitigation factor.

The role of tree roots in soil stabilisation has been widely studied, with research demonstrating that root systems contribute significantly to mechanical reinforcement, particularly on unstable or sloped terrain (Schwarz et al., 2010). Similarly, studies on slope stability (Schwarz et al., 2013, 2016) have demonstrated that tree roots increase shear strength and reduce lateral soil movement. This may explain why stumps have a stronger influence on rut depth in curved trails, where lateral soil displacement is greater.

While the stabilising effect of roots has been well-documented, fewer studies have explored how stump-root systems change soil deformation in forestry operations. Piskunov (2023) found that stump-root systems significantly reduced rut depth, with effects strongest within 0.5 to 1.5 meters from the stump. This supports the idea that stumps serve as natural reinforcements, with their impact gradually diminishing with distance (Schwarz et al., 2010). However, previous studies have not incorporated spatial modelling to quantify these effects across larger areas, leaving a gap in understanding how stump influence varies across different terrains and machine traffic patterns.

While this study offers useful insights, some limitations should be noted. UAV-based measurements, though effective, underestimated deeper ruts, particularly in curved trails, likely due to the averaging effect within the 10 cm buffer and interpolation errors. Future research could enhance accuracy by incorporating LiDAR to capture fine-scale variations in rut depth.

The study's focus on a single peatland site may limit the generalisability of the results. Peat soils have unique properties, such as high organic content and water saturation, which may not be representative of mineral soils or drier forest conditions (Laine et al., 2006; Paavilainen & Päivänen, 1995; Sallinen et al., 2019). Expanding research to include diverse soil types and forest ecosystems would be necessary for broader applicability and to determine whether stump effects vary across ecological conditions.

Another limitation concerns parameter (CI, RRV) modelling. In this study, we employed simplified spatial modelling techniques using UAV data and other parameters to quantify how stump presence affects rut formation. We presumed that reinforcement strength slowly diminishes as the distance from the stump grows (Schwarz et al., 2010). Although this offers a more straightforward method for representing root-soil interactions, it fails to accurately present the true spatial arrangement of root systems. Under real-world conditions, root expansion is inconsistent, differing based on species, soil types, and the age of the tree. Roots do not grow uniformly in every direction (Kalliokoski, 2011), suggesting that presuming a consistent, symmetrical decrease in reinforcement around the entire stump may lead to some level of overgeneralisation. Also, calculating actual root reinforcement values is highly complex and typically requires extensive fieldwork and laboratory tests to measure parameters such as root tensile strength, RAR, soil shear strength, and root distribution (Genet et al., 2005; Schwarz et al., 2010; Van Beek et al., 2007). Although our method establishes a useful experimental baseline, it might fail to fully reflect the unique root architecture of different species or the mechanical characteristics of specific root systems. Future studies might improve model precision by developing species-specific constants for root reinforcement assessments, particularly for economically significant species like Scots pine and Norway spruce. This could be accomplished by integrating field-based root mapping, which might help in creating species-specific root spread patterns. Techniques like ground-penetrating radar (GPR) have already been successfully employed in ecological and geotechnical studies to identify and obtain three-dimensional visualisation of shallow and deep tree root systems (Alani et al., 2018).

The stabilising influence of stumps on soil support, particularly in reducing rut formation, highlights their critical role in sustainable forest operations. By incorporating stump-related variables into predictive models, forest managers can improve rut depth forecasting and optimise operational planning, minimise soil disturbances and improve both economic and ecological outcomes. These models can help identify optimal skid trails and sensitive areas to avoid, reducing unnecessary machine movements and lowering the risk of equipment damage. This approach could further improve planning efficiency and reduce operational costs. However, as the current approach to root reinforcement modelling remains simplified, methodological improvements are necessary. These advancements will contribute to more sustainable forest management practices, balancing operational efficiency with ecological preservation.

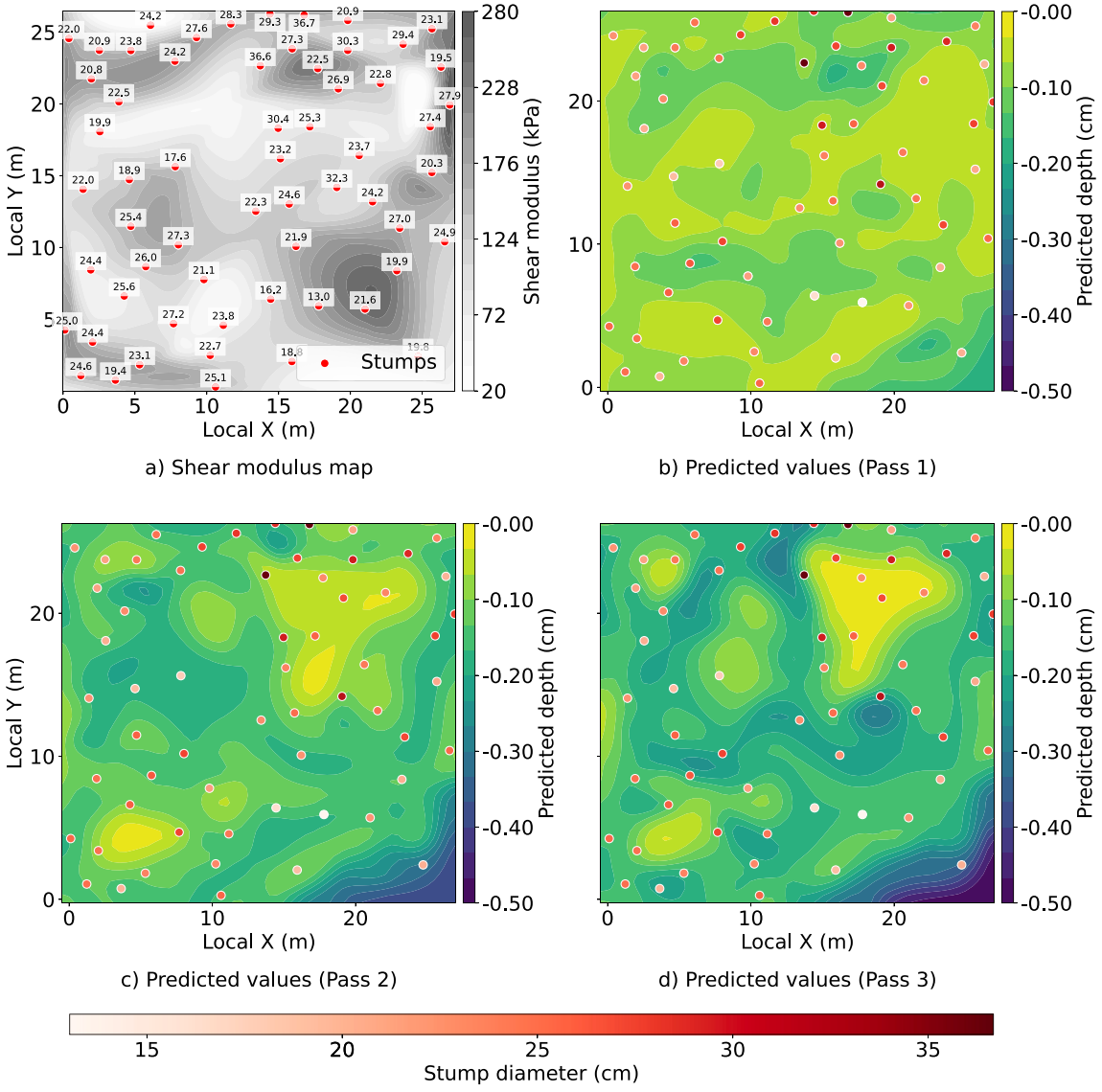

Fig. 10. Spatial visualisation of shear modulus and predicted rut depth (cm) across multiple passes using a Random Forest (RF) model. Figure (a) presents a synthetic shear modulus map (in kPa) generated from randomly placed control points and interpolated across the area, overlaid with synthetic tree stumps (red dots). Figure (b–d) show predicted rut depth values (for Passes 1, 2, and 3) using root reinforcement value (RRV), cumulative unfluence (CI), and shear modulus (G_{trail}) as predictors. The colour bar at the bottom represents the stump diameter (cm) and applies only to the red stump symbols. Each pass visualises rut depths in conjunction with stump locations. (For interpretation of the references to colour in this figure legend, the reader is referred to the web version of this article.)

5. Conclusion

This study demonstrated that stump presence plays an important role in reducing rut formation on peatland soils, with effects varying by trail configuration. Using UAV-based measurements, statistical analysis, spatial modelling, and machine learning, we highlight the role of biological reinforcement in mitigating machine-induced soil deformation. The RF model identified stump presence, reinforcement effects, and shear modulus as key predictors of rut depth, demonstrating the combined impact of biological and mechanical soil properties.

Integrating stump influence into rut depth prediction models can improve machine path planning and soil conservation in peatland forestry. However, site-specific conditions and the simplified nature of current reinforcement modelling suggest that species-specific constants and advanced mapping techniques, such as GPR, could improve accuracy. Future research should refine root reinforcement models, integrate high-resolution root mapping, and expand to diverse soil types to improve predictive accuracy and support sustainable forest management.

CRediT authorship contribution statement

Gunta Grube: Writing – review & editing, Writing – original draft, Visualization, Validation, Software, Methodology, Investigation, Formal analysis, Data curation, Conceptualization. **Stefano Grigolato:** Writing – review & editing, Supervision, Project administration, Funding acquisition, Conceptualization. **Jari Ala-Ilomäki:** Writing – review & editing, Data curation, Conceptualization. **Johanna Routa:** Writing – review & editing, Data curation. **Harri Lindeman:** Writing – review & editing, Data curation, Conceptualization. **Rasmus Astrup:** Writing – review & editing, Project administration, Funding acquisition, Data curation, Conceptualization. **Bruce Talbot:** Writing – review & editing, Methodology, Investigation, Data curation, Conceptualization.

Disclosure on the use of AI in scientific writing

During the preparation of this work, the author(s) used Perplexity AI (GPT-4.5 model) to assist with language refinement and coding tasks, particularly in generating plots and LaTeX tables. After using this

tool/service, the author(s) reviewed and edited the content as needed and take(s) full responsibility for the content of the publication.

Declaration of competing interest

The authors declare that they have no known competing financial interests or personal relationships that could have appeared to influence the work reported in this paper.

Acknowledgements

This research was supported by the Horizon 2020 European Union Funding for Research and Innovation under the Marie Skłodowska-Curie Actions of the main programme "Excellent Science", project Skill-For.Action (Grant Agreement No. 956355), the Agritech National Research Center and the European Union NextGenerationEU (PIANO NAZIONALE DI RIPRESA E RESILIENZA (PNRR) – MISSIONE 4 COMPONENTE 2, INVESTIMENTO 1.4 – D.D. 1032 17/06/2022) (Grant Agreement No. CN00000022), and Bio-Based Industries Joint Undertaking under the European Union's Horizon 2020 research and innovation program, TECH4EFFECT- Knowledge and Technologies for Effective Wood Procurement - project (grant number 720757). The authors would also like to express their gratitude to Dr. Robert Prinz (Natural Resources Institute Finland, Finland), Dr. Kari Väätäinen (Natural Resources Institute Finland, Finland), Dr. Simon Berg (NIBIO, Norway), and Tyrone Nowell (NIBIO, Norway) for their contributions and support in field data collection.

Data availability

Data are available on request.

References

Agisoft, L. (2021). Agisoft metashape user manual: Professional edition, version 1.7. Retrieved from https://www.agisoft.com/pdf/metashape-pro_1_7_en.pdf.

Ala-Ilomäki, J. (2013). Spiked shear vane—A new tool for measuring peatland top layer strength. *Mires and Peat*, *64*(2–3), 113–118.

Ala-Ilomäki, J., Högnäs, T., Lamminen, S., & Sirén, M. (2011). Equipping a conventional wheeled forwarder for peatland operations. *International Journal of Forest Engineering*, *22*(1), 7–13.

Ala-Ilomäki, J., Lindeman, H., Mola-Yudego, B., Prinz, R., Väätäinen, K., Talbot, B., & Routa, J. (2021). The effect of bogie track and forwarder design on rut formation in a peatland. *International Journal of Forest Engineering*, *32*(sup1), 12–19.

Alani, A. M., Ciampoli, L. B., Lantini, L., Tosti, F., & Benedetto, A. (2018). Mapping the root system of matured trees using ground penetrating radar. In *2018 17th international conference on ground penetrating radar* (pp. 1–6). IEEE.

Bhatnagar, S., Puliti, S., Talbot, B., Heppelmann, J. B., Breidenbach, J., & Astrup, R. (2022). Mapping wheel-ruts from timber harvesting operations using deep learning techniques in drone imagery. *Forestry*, *95*(5), 698–710.

Blattert, C., Mönkkönen, M., Burgas, D., Di Fulvio, F., Toraño Caicoya, A., Vergarechea, M., Klein, J., Hartikainen, M., Antón-Fernández, C., Astrup, R., et al. (2023). Climate targets in European timber-producing countries conflict with goals on forest ecosystem services and biodiversity. *Communications Earth & Environment*, *4*(1), 119.

Breiman, L. (2001). Random forests. *Machine Learning*, *45*, 5–32.

Breinig, L., Hinte, B., Schönauer, M., Hoffmann, S., Brokmeier, H., & Jaeger, D. (2025). Traction assistance of a forwarder in flat terrain: Effects on wheel slip and soil disturbance. *Croatian Journal of Forest Engineering: Journal for Theory and Application of Forestry Engineering*, *46*(1), 1–17.

Brennensthul, M., Czarnecki, J., & Białczyk, W. (2024). Assessment of tractor tires used in forest conditions in terms of traction performance and impact on ground. *Croatian Journal of Forest Engineering: Journal for Theory and Application of Forestry Engineering*, *45*(1), 97–114.

Carroll, R. M., & Nordholm, L. A. (1975). Sampling characteristics of Kelley's ε and Hays' ω. *Educational and Psychological Measurement*, *35*(3), 541–554.

CloudCompare (2024). CloudCompare (version 2.13.2) [computer software]. Retrieved April 3, 2024. http://www.cloudcompare.org/.

Coutts, M. P. (1983). Root architecture and tree stability. In D. Atkinson, K. K. S. Bhat, M. P. Coutts, P. A. Mason, & D. J. Read (Eds.), *Tree root systems and their mycorrhizas* (pp. 171–188). Dordrecht: Springer Netherlands, http://dx.doi.org/10.1007/978-94-009-6833-2_18.

Favero, A., Daigneault, A., & Sohngen, B. (2020). Forests: Carbon sequestration, biomass energy, or both? *Science Advances*, *6*(13), eaay6792. http://dx.doi.org/10.1126/sciadv.aay6792.

Finnish Meteorological Institute (2018). Climate in Finland. Retrieved from https://en.ilmatieteenlaitos.fi/climate. (Accessed 11 July 2024).

Genet, M., Stokes, A., Salin, F., Mickovski, S. B., Fourcaud, T., Dumail, J.-F., & Van Beek, R. (2005). The influence of cellulose content on tensile strength in tree roots. *Plant and Soil*, *278*, 1–9.

Glass, G. V., & Hakstian, A. R. (1969). Measures of association in comparative experiments: Their development and interpretation. *American Educational Research Journal*, *6*(3), 403–414.

Grassi, G., House, J., Dentener, F., Federici, S., den Elzen, M., & Penman, J. (2017). The key role of forests in meeting climate targets requires science for credible mitigation. *Nature Climate Change*, *7*(3), 220–226.

Heppelmann, J., Talbot, B., Antón Fernandéz, C., & Astrup, R. (2022). Depth-to-water maps as predictors of rut severity in fully mechanized harvesting operations. *International Journal of Forest Engineering*, *33*(2), 108–118.

Kalliokoski, T. (2011). Root system traits of Norway spruce, scots pine, and silver birch in mixed boreal forests: an analysis of root architecture, morphology, and anatomy. *Dissertationes Forestales*, *121*, 67.

Laine, J., Laiho, R., Minkkinen, K., & Vasander, H. (2006). Forestry and boreal peatlands. *Boreal Peatland Ecosystems*, 331–357.

Lepilin, D., Laurén, A., Uusitalo, J., Fritze, H., Laiho, R., Kimura, B., & Tuittila, E.-S. (2022). Response of vegetation and soil biological properties to soil deformation in logging trails of drained boreal peatland forests. *Canadian Journal of Forest Research*, *52*(4), 511–526.

Lerink, B. J., Schelhaas, M.-J., Schreiber, R., Aurenhammer, P., Kies, U., Vuillermoz, M., Ruch, P., Pupin, C., Kitching, A., Kerr, G., et al. (2023). How much wood can we expect from European forests in the near future? *Forestry: An International Journal of Forest Research*, *96*(4), 434–447.

Loisel, J., & Gallego-Sala, A. (2022). Ecological resilience of restored peatlands to climate change. *Communications Earth & Environment*, *3*(1), 208.

Marra, E., Wictorsson, R., Bohlin, J., Marchi, E., & Nordfjell, T. (2021). Remote measuring of the depth of wheel ruts in forest terrain using a drone. *International Journal of Forest Engineering*, *32*(3), 224–234.

Masi, E. B., Segoni, S., & Tofani, V. (2021). Root reinforcement in slope stability models: a review. *Geosciences*, *11*(5), 212.

Miljøministeriet (2005). Miljøkrav til skovmaskiner på skov- og naturstyrelsens arealer [environmental requirements for forestry machines on forest and nature agency lands]. Retrieved December 18, 2024. https://naturstyrelsen.dk/media/ysdnrry5/bilag7miljkrav_skovmaskiner2005.pdf.

Neri, F., Spinelli, R., & Lyons, J. (2007). Ground pressure forwarder trials: Assess benefits in reducing wheel rutting. In *Austro2007/fORMEC'07: meeting the needs of tomorrows' forests – new developments in forest engineering, Vienna and Heiligenkreuz, Austria, October 7–11, 2007* (pp. 1–10). URL https://www.formec.org/images/proceedings/2007/session_5_pdf/5_2_paper_neri_spinelli_lyons_austro_formec_2007.pdf.

Nevalainen, P., Salmivaara, A., Ala-Ilomäki, J., Launiainen, S., Hiedanpää, J., Finér, L., Pahikkala, T., & Heikkonen, J. (2017). Estimating the rut depth by UAV photogrammetry. *Remote Sensing*, *9*(12), 1279.

Niemi, M. T., Vastaranta, M., Vauhkonen, J., Melkas, T., & Holopainen, M. (2017). Airborne LiDAR-derived elevation data in terrain trafficability mapping. *Scandinavian Journal of Forest Research*, *32*(8), 762–773.

Paavilainen, E., & Päivänen, J. (1995). Utilization of peatlands. In *Peatland forestry: ecology and principles* (pp. 15–29). Berlin, Heidelberg: Springer, http://dx.doi.org/10.1007/978-3-662-03125-4_2.

Pedregosa, F., Varoquaux, G., Gramfort, A., Michel, V., Thirion, B., Grisel, O., Blondel, M., Prettenhofer, P., Weiss, R., Dubourg, V., et al. (2011). Scikit-learn: Machine learning in python. *Journal of Machine Learning Research*, *12*, 2825–2830.

Peltola, A. (2014). *Metsätilastollinen vuosikirja 2014: Finnish Statistical Yearbook of Forestry 2014*. Vantaa, Finland: Metsäntutkimuslaitos (Metla), URL https://www.metla.fi/julkaisut/metsatilastollinenvsk/2014/index.htm. Retrieved April 3, 2024.

Piirainen, S., Finér, L., Andersson, E., Armolaitis, K., Belova, O., Čiuldienė, D., Futter, M., Gil, W., Glazko, Z., Hiltunen, T., Högbom, L., Janek, M., Joensuu, S., Jägrud, L., Libiete, Z., Lode, E., Löfgren, S., Pierzgalski, E., Sikström, U., ... Thorell, D. (2017). *Forest Drainage and Water Protection in the Baltic Sea Region Countries – Current Knowledge, Methods and Areas for Development: Technical report*, Interreg Baltic Sea Region, European Regional Development Fund, URL https://www.skogsstyrelsen.se/globalassets/projektwebbplatser/wambaf/drainage/reviews/forest-drainage_short_document_imposed_21032017.pdf.

Piskunov, M. (2023). Influence of stump-root system of trees on rut formation during forwarder operation on peat soils. *Croatian Journal of Forest Engineering: Journal for Theory and Application of Forestry Engineering*, *44*(2), 217–231.

Prinz, R., Mola-Yudego, B., Ala-Ilomäki, J., Väätäinen, K., Lindeman, H., Talbot, B., & Routa, J. (2023). Soil, driving speed and driving intensity affect fuel consumption of forwarders. *Croatian Journal of Forest Engineering: Journal for Theory and Application of Forestry Engineering*, *44*(1), 31–43.

Roberts, R., Inzerillo, L., & Di Mino, G. (2020). Using UAV based 3D modelling to provide smart monitoring of road pavement conditions. *Information*, *11*(12), 568.

Sallinen, A., Tuominen, S., Kumpula, T., & Tahvanainen, T. (2019). Undrained peatland areas disturbed by surrounding drainage: a large scale GIS analysis in Finland with a special focus on aapa mires. *Mires and Peat*, *24*, 38.

Schwarz, M., Giadrossich, F., & Cohen, D. (2013). Modeling root reinforcement using a root-failure Weibull survival function. *Hydrology and Earth System Sciences*, *17*(11), 4367–4377.

Schwarz, M., Lehmann, P., & Or, D. (2010). Quantifying lateral root reinforcement in steep slopes–from a bundle of roots to tree stands. *Earth Surface Processes and Landforms: The Journal of the British Geomorphological Research Group*, *35*(3), 354–367.

Schwarz, M., Phillips, C., Marden, M., McIvor, I., Douglas, G., & Watson, A. (2016). Modelling of root reinforcement and erosion control by 'Veronese'poplar on pastoral hill country in New Zealand. *New Zealand Journal of Forestry Science*, *46*, 1–17.

Similä, M., Aapala, K., & Penttinen, J. (Eds.), (2014). *Ecological Restoration in Drained Peatlands: Best Practices from Finland*. Vantaa, Finland: Metsähallitus, Natural Heritage Services.

Solgi, A., Naghdi, R., Labelle, E. R., & Zenner, E. K. (2018). The effects of using soil protective mats of varying compositions and amounts on the intensity of soil disturbances caused by machine traffic. *International Journal of Forest Engineering*, *29*(3), 199–207.

Stokes, A., & Mattheck, C. (1996). Variation of wood strength in tree roots. *Journal of Experimental Botany*, *47*(5), 693–699.

Turunen, J., & Valpola, S. (2020). The influence of anthropogenic land use on finnish peatland area and carbon stores 1950–2015. *Mires and Peat*, *26*, 27.

Uusitalo, J., & Ala-Ilomäki, J. (2013). The significance of above-ground biomass, moisture content and mechanical properties of peat layer on the bearing capacity of ditched pine bogs. *Silva Fennica*, *47*(3).

Uusitalo, J., Salomäki, M., & Ala-Ilomäki, J. (2015). The effect of wider logging trails on rut formations in the harvesting of peatland forests. *Croatian Journal of Forest Engineering: Journal for Theory and Application of Forestry Engineering*, *36*(1), 125–130.

Van Beek, L. P. H., Wint, J., Cammeraat, L. H., & Edwards, J. P. (2007). Observation and simulation of root reinforcement on abandoned Mediterranean slopes. In *Eco- and ground bio-engineering: the use of vegetation to improve slope stability. proceedings of the first international conference on eco-engineering, 13–17 September 2004* (pp. 91–109). Springer.

Vega-Nieva, D. J., Murphy, P. N., Castonguay, M., Ogilvie, J., & Arp, P. A. (2009). A modular terrain model for daily variations in machine-specific forest soil trafficability. *Canadian Journal of Soil Science*, *89*(1), 93–109.

Waldron, L. (1977). The shear resistance of root-permeated homogeneous and stratified soil. *Soil Science Society of America Journal*, *41*(5), 843–849.

Wästerlund, I. (1989). Strength components in the forest floor restricting maximum tolerable machine forces. *Journal of Terramechanics*, *26*(2), 177–182.

Wu, T. H., McKinnell III, W. P., & Swanston, D. N. (1979). Strength of tree roots and landslides on prince of Wales island, Alaska. *Canadian Geotechnical Journal*, *16*(1), 19–33.

Zhang, W., Qi, J., Wan, P., Wang, H., Xie, D., Wang, X., & Yan, G. (2016). An easy-to-use airborne LiDAR data filtering method based on cloth simulation. *Remote Sensing*, *8*(6), 501.

Zoltai, S. C., Martikainen, P. J., et al. (1996). Estimated extent of forested peatlands and their role in the global carbon cycle. In *NATO ASI Series I: Global Environmental Change*: *Vol. 40*, (pp. 47–58). Springer.